## Supporting Information

# SURVIVAL AND DIVERGENCE IN A SMALL GROUP: THE EXTRAORDINARY GENOMIC HISTORY OF THE ENDANGERED APENNINE BROWN BEAR

Andrea Benazzo[a,*], Emiliano Trucchi[a,b,*], James A. Cahill[c], Pierpaolo Maisano Delser[d,e,f], Stefano Mona[d,e], Matteo Fumagalli[g], Lynsey Bunnefeld[h,i], Luca Cornetti[j], Silvia Ghirotto[a], Matteo Girardi[k], Lino Ometto[l,m], Alex Panziera[a], Omar Rota-Stabelli[l], Enrico Zanetti[a], Alexandros Karamanlidis[n], Claudio Groff[o], Ladislav Paule[p], Leonardo Gentile[q], Carles Vilà[r], Saverio Vicario[s], Luigi Boitani[t], Ludovic Orlando[u], Silvia Fuselli[a], Cristiano Vernesi[k], Beth Shapiro[c], Paolo Ciucci[t], Giorgio Bertorelle[a,1].

[a]Department of Life Sciences and Biotechnology, University of Ferrara, 44121 Ferrara, Italy
[b]Centre for Ecological and Evolutionary Synthesis (CEES), Department of Biosciences, University of Oslo, Oslo 1066, Norway
[c]Department of Ecology and Evolutionary Biology, University of California, Santa Cruz, CA 95064, USA
[d]Institute de Systematics, Evolution, Biodiversite, ISYEB-UMR 7205-CNRS, MNHN, UPMC, EPHE, Ecole Pratique de Hautes Etudes, CP39, 75005, Paris, France
[e]EPHE, PSL Research University, 75005, Paris, France
[f]Smurfit Institute of Genetics, University of Dublin, Trinity College, Dublin 2, Ireland.
[g]Department of Life Sciences, Silwood Park Campus, Imperial College London, Ascot, SL5 7PY, United Kingdom
[h]Institute of Evolutionary Biology, University of Edinburgh, Edinburgh, EH9 3FL, United Kingdom
[i]Biological and Environmental Science, University of Stirling, Stirling, FK9 4LA, United Kingdom
[j]Zoological Institute, University of Basel, 4051, Basel, Switzerland
[k]Department of Biodiversity and Molecular Ecology, Fondazione Edmund Mach, 38010, San Michele all'Adige, Italy
[l]Department of Sustainable Agro-ecosystems and Bioresources, Fondazione Edmund Mach, 38010, San Michele all'Adige, Italy
[m]Independent researcher, 38016, Mezzocorona, Italy
[n]ARCTUROS, Protection and Management of Wildlife and the Natural Environment, 53075 Aetos, Florina, Greece
[o]Provincia Autonoma di Trento, 38100, Trento, Italy
[p]University of Technology, 96001, Zvolen, Slovakia
[q]Veterinary Service, National Park of Abruzzo Lazio and Molise, 67032 Pescasseroli, Italy
[r]Doñana Biological Station (EBD-CSIC), 4102 Seville, Spain
[s]Institute of Atmospheric Pollution Research and Technologies, National Research Council, 70126, Bari, Italy
[t]Department of Biology and Biotechnologies 'Charles Darwin', University of Rome La Sapienza, 00185 Rome, Italy
[u]Centre for GeoGenetics, Natural History Museum of Denmark, University of Copenhagen, 1350 K Copenhagen, Denmark

[1]*Corresponding author:* Giorgio Bertorelle, Department of Life Sciences and Biotechnology, University of Ferrara, via Borsari 46, 44121, Ferrara, Italy. Phone: +390532455743. Email:ggb@unife.it
[*]*Equally contributing authors*

**Table of contents**

**Author contributions**

GB headed the project
GB, AB, PC and LB initially conceived the project
AB, ET, and JC performed most the bioinformatics and population genomics analyses
PMD and SM developed and tested the ABC models
MF performed the inbreeding analyses
SG performed the Structure analysis
ORS performed the phylogenetic analyses
LC, AP, SF, LO, SV, and EZ contributed to the selection analyses
MG, JC, BS, SF, and CVe performed laboratory analyses
PC, CVe, CVi, CG, AK, LP provided samples
GB wrote the manuscript, with input from ET and all the other authors
All the authors discussed and approved the final version of the manuscript

**Supplementary Figures**

**Supplementary Tables**

## S1 Sampling, genome sequencing and pattern of variation

### S1.1 Short description of the Apennine brown bear

Current population size of brown bear in the Central Apennines is about 50 individuals of all ages (1), plus a few erratic individuals with little, if any, demographic value. The reproductive portion of the population is restricted to the core range, corresponding to the Abruzzo, Lazio, and Molise National Park and its contiguous areas (Fig. S1), for about 1500 $km^2$ (2). The extension of the peripheral area with occasional bear occurrence is about 5,500 $km^2$ if we also consider an isolated northernmost fringe in the Monti Sibillini National Park (approximately 100 km northern of the core range), where only a single male has been observed over a 2006-2010 survey (2). The Apennine population is therefore separated from the closest population in the Alps by >400 km and the large unsuitable plain crossed by the river Po. A study describing occasional bear occurrence in the peripheral area (see Fig. 2 in (2)) shows approximately 300 tracks and sightings, recorded between 2000 and 2014 (3), but the number of individuals was not estimated and only 3 records of females with cubs were further validated (2). All in all, the occasional occurrence of bears outside the core area has been related to seasonally wandering individuals (usually males), or unsuccessful attempts of re-colonization, and there is no evidence of a stable population in these marginal areas (2). Historical records indicate that the distribution of the Apennine brown bear in the last few centuries was wider than today, but it did not extend northern of the Sibillini mountains (4).

Age at first reproduction in females varies from 4 to 6 years, and interbirth interval averages 3.7 years. Each reproductive female produces 1-2 cubs, rarely 3, and weaning occurs during the second year of a cub's life (5). The Apennine bear population is reproductively active and demographically stable (6). Estimates of survival in adults, litter size, and interbirth interval are in line with values reported for other brown bear populations in Europe and North America (5, 6). The estimated cub survival (0.51) is in the first quartile of the distribution of values observed in 16 non-hunted populations (min = 0.34; max = 0.91), but its 95% confidence interval (0.22 - 0.79) is large. Reproductive traits require further investigations (6).

Brown bears in the Central Apennines are relatively smaller compared to other European brown bear populations. For example, adult males average approximately 190 kg (P. Ciucci, pers. comm.), whereas the weight in other populations in northern and southern Europe varies between 200 and 250 kg (7). The sexual dimorphism in Apennine bears is particularly evident in the shape of the skull (8). Their diet is prevalently composed of vegetable matter, including herbs and forbs in the spring, followed by a variety of soft fruit in the summer and hard mast in autumn, even though animal proteins are actively sought through consumption of ants in early summer, wild herbivores in spring, and livestock remains throughout the year (9). Apennine bears are not known to actively predate large ungulates, but their remains are found in scats and predation on roe deer fawns and wild boar piglets cannot be excluded (1). A few individuals, usually large adult males, do actively predate livestock, mainly unattended sheep and calves. Apennine bears prefer areas located at high elevation and in densely forested sites.

**Fig. S1. Distribution of the Apennine brown bear reproductive population.** This figure is based on 22828 location data (sightings of bear family groups, telemetry, and non invasive genetic relocations of 7 marked females known to have produced cubs) collected between 2005 and 2014 (light yellow shade; modified from Fig. 2 in Ref. 2). Peripheral area where mostly wandering male individuals have been observed is shown (gray shade). Twelve Apennine brown bear samples analyzed in this study: nuclear and mitochondrial genome sequences available (solid red circle), only mitochondrial genome sequence available (empty red circle). Administrative regional boundaries (thin gray line) and highways (thick gray line) are indicated.

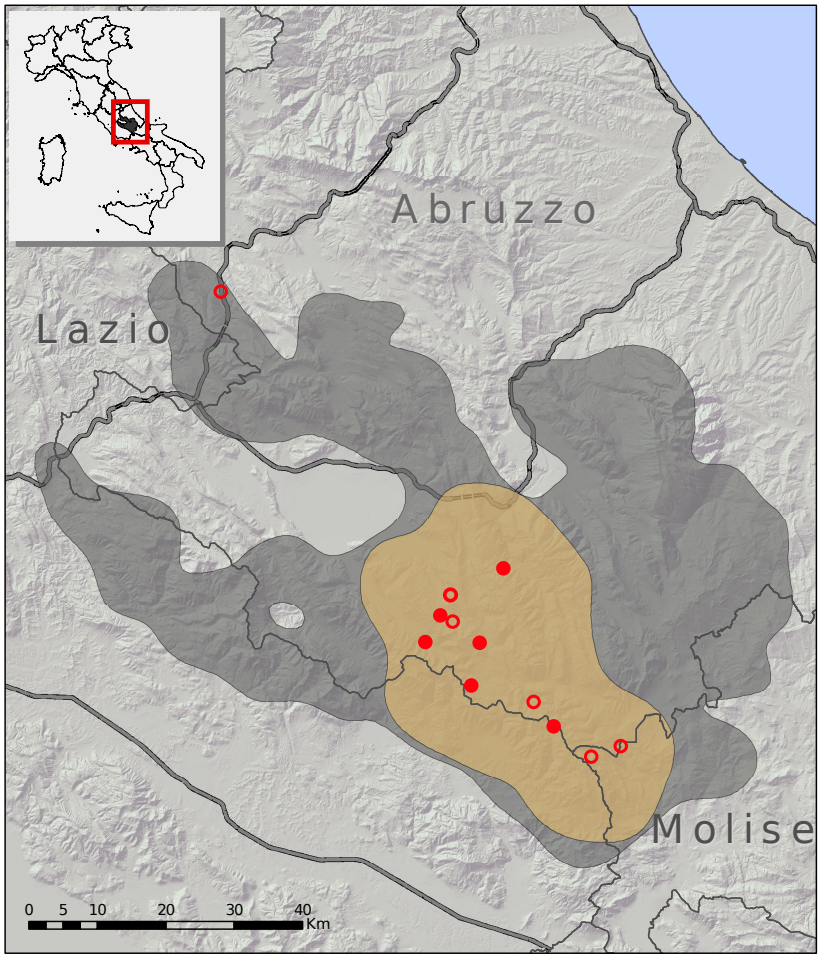

**Table S1**. **Samples employed in this study, with SRA Accession Numbers (BioProject: PRJNA395974)**. Genome sequences downloaded from public repository and referenced in previously published studies are indicated. No brown bears from America were used to avoid possible admixture issues (10). Sampling localities of Apennine brown bear are shown in Fig. S1.

| Sample ID | Color code | Accession/Reference | Species | Origin | Gender | Coverage |
|---|---|---|---|---|---|---|
| APN1 | | SRR5878361 (raw reads), SRR5878350 (mapped reads) | *U. arctos* | Central Italy | F | LOW |
| APN2 | | SRR5878360 (raw reads), SRR5878348 (mapped reads) | *U. arctos* | Central Italy | M | HIGH |
| APN3 | | SRR5878359 (raw reads), SRR5878343 (mapped reads) | *U. arctos* | Central Italy | M | LOW |
| APN4 | | SRR5878358 (raw reads), SRR5878342 (mapped reads) | *U. arctos* | Central Italy | F | LOW |
| APN5 | | SRR5878357 (raw reads), SRR5878345 (mapped reads) | *U. arctos* | Central Italy | M | LOW |
| APN6 | | SRR5878356 (raw reads), SRR5878344 (mapped reads) | *U. arctos* | Central Italy | F | LOW |
| GRE1 | | SRR5878355 (raw reads), SRR5896131 (mapped reads) | *U. arctos* | Greece | M | LOW |
| GRE2 | | SRR5878354 (raw reads), SRR5878351 (mapped reads) | *U. arctos* | Greece | M | LOW |
| SLK1 | | SRR5878353 (raw reads), SRR5878338 (mapped reads) | *U. arctos* | Slovakia | M | HIGH |
| SLK2 | | SRR5878349 (raw reads), SRR5878339 (mapped reads) | *U. arctos* | Slovakia | M | LOW |
| SPA1 | | SRR5878347 (raw reads), SRR5878340 (mapped reads) | *U. arctos* | NW Spain | M | HIGH |
| ALP1 | | SRR5878346 (raw reads), SRR5878341 (mapped reads) | *U. arctos* | N Italy | F | HIGH |
| SWE1 | | grz3 (11) | *U. arctos* | S Sweden | F | HIGH |
| SWE2 | | grz4 (11) | *U. arctos* | N Sweden | F | HIGH |
| POL1 | | pb28 (11) | *U. maritimus* | E Greenland | F | HIGH |
| POL2 | | pb7a (11) | *U. maritimus* | E Greenland | F | HIGH |
| POL3 | | pb3 (12) | *U. maritimus* | E Greenland | F | HIGH |
| POL4 | | pb105 (11) | *U. maritimus* | W Greenland | F | HIGH |
| POL5 | | pb12 (11) | *U. maritimus* | W Greenland | F | HIGH |
| POL6 | | pb68 (11) | *U. maritimus* | W Greenland | F | HIGH |
| BLK1 | | blk (12) | *U. americanus* | Alaska | M | HIGH |

**S1.2 Sample preparation and whole-genome sequencing**

Genomic DNA has been extracted from blood and muscle tissue following the manufacturer's instruction of the Omega-Biotek (Norcross, USA) Mag-Bind Blood & Tissue kit. DNA concentration was determined using Qubit fluorometer with the High Sensitivity dsDNA kit (Thermo-Fisher, USA).

Samples were prepared for paired-end Illumina sequencing following the protocol described in (13). Briefly, we sonicated 500 ng of DNA, which we then end-polished to create blunt ends, and size-selected with Ampure beads to an average size of approximately 275 bp. Next, we ligated hemi-single-stranded Illumina-compatible sequencing adapters and purified the DNA on solid phase reversible illumination (SPRI) beads. We filled-in the adapters with Bst DNA polymerase (NEB), followed by a second purified on SPRI beads. We then performed Indexing PCR with KOD DNA polymerase (EMD Millipore #71086), purified the resulting products on SPRI beads, and performed size selection on an E-gel (ThermoFisher) to remove adapter dimers and refine the insert range of the library. Library quality and complexity was assessed via low-coverage sequencing on an Illumina Miseq. Libraries that were selected for deeper sequencing were then pooled in equimolar ratios and paired-end sequencing (2x100) using an Illumina HiSeq 2000 in high output mode at the Vincent J. Coates Sequencing Facility at UC Berkeley.

**S1.3 Mapping the reads to the polar bear reference genome**

All reads sequenced in this study were processed with *SeqPrep* (https://github.com/jstjohn/SeqPrep) to remove Illumina adapters and merge overlapping reads. Paired-end and merged reads were then aligned to the polar bear genome (11) using the *aln* algorithm implemented in the *bwa v0.6.2* aligner (14) using default parameters. Alignments were filtered excluding reads with mapping quality lower than 25, sorted and indexed using *samtools v0.1.19* (15). PCR duplicates, produced by the amplification step during library preparation, were removed using the *rmdup* tool in the *samtools* package. Sites near indel showing putative alignment errors were marked and realigned using the *RealignerTargetCreator* and the *IndelRealignment* tools in *GATK* (16).

We included in our analyses European (Sweden) brown bear, polar bear and black bear data from previously published studies (11, 12). We downloaded paired-end reads from GenBank (BLK: SRR518723; GRZ4: SRR935627, SRR935625, SRR935591; GRZ3: SRR935626, SRR935593, SRR935594, SRR935590; PB3: SRR518672, SRR518673; PB105: SRR947747, SRR942284, SRR942285; PB28: SRR942295, SRR942287, SRR942211; PB7a: SRR942299, SRR942291, SRR942218; PB12: SRR942301, SRR942293, SRR942260; PB68: SRR942302, SRR942294, SRR942240) and applied the same informatics pipeline as outlined above without merging the overlapping reads. A small portion (<5%) of the reference polar bear genome is composed by thousands of very short fragments (<200bp) which are not suitable for many population genetic analyses. We then excluded all fragments shorter than 100kb and retained as reference genome a set of 371 long scaffolds representing 95.3% of the genome. Based on the literature, we could associate 2 scaffolds (~627kb) to the Y chromosome (17) and 12 scaffold (~73.5Mb) to the X chromosome (10) whereas the remaining 357 scaffolds were considered to come from autosomes (~2.16Gb).

We produced a total of ~2.14 billion reads uniquely mapping to the polar bear genome with a high confidence (Q>=25). The amount of reads aligned to autosomal scaffolds, the proportion of the genome covered by at least one read and the mean coverage for each individual is reported in Table S2. All individuals showed a high proportion of the genome covered by reads (from 95.29% to 99.84%) except APN1 sample for which the proportion dropped to 90.89%. Eight individuals were sequenced at low coverage with an average sequencing depth from 2.4 to 6.3X, whereas four remaining individuals were sequenced at higher coverage (from 14.4 to 16.5X). Two brown and six polar bears sequenced in previous

studies (add reference) showed an average depth ranging from 16.2 to 29.8X. We then analyzed a high coverage dataset including six brown bear individuals from Central Italy (i.e. Apennine brown bear), Northern Italy, Spain, Slovakia, North and South Sweden, six polar bear individuals (Greenland) and one black bear individual (Alaska, US). The high coverage dataset was further integrated with four low coverage samples from Central Italy (i.e. Apennine brown bear), two from Greece and one from Slovakia in some of the downstream analyses (see details below). The APN1 sample was excluded from the analysis due to its low coverage and small proportion of genome sequenced.

**Table S2. Coverage summary statistics of whole-genome sequences employed in this study.**

| Sample ID | Reads aligned to the polar bear genome | Proportion of the genome covered (%) | Mean coverage |
|---|---|---|---|
| APN1 | 55,009,465 | 90.89 | 2.4 |
| APN2 | 312,727,267 | 98.81 | 14.41 |
| APN3 | 135,675,928 | 98.32 | 5.7 |
| APN4 | 88,021,067 | 96.61 | 3.8 |
| APN5 | 76,662,120 | 95.29 | 3.2 |
| APN6 | 141,761,683 | 98.44 | 6.3 |
| GRE1 | 95,370,878 | 97.39 | 4.4 |
| GRE2 | 144,668,979 | 98.31 | 6.1 |
| SLK1 | 301,679,784 | 98.82 | 14.6 |
| SLK2 | 123,613,393 | 98.19 | 5.2 |
| SPA1 | 347,854,696 | 98.86 | 16.57 |
| ALP1 | 316,725,859 | 98.84 | 14.86 |
| SWE1 | 629,987,493 | 99.75 | 23.8 |
| SWE2 | 434,930,984 | 99.67 | 16.3 |
| POL1 | 776,380,905 | 99.84 | 29.8 |
| POL2 | 707,880,035 | 99.38 | 28.0 |
| POL3 | 394,584,834 | 99.24 | 16.2 |
| POL4 | 725,135,601 | 99.38 | 29.3 |
| POL5 | 635,536,602 | 99.36 | 23.7 |
| POL6 | 717,410,063 | 99.37 | 29.1 |
| BLK1 | 572,061,050 | 99.72 | 20.7 |

**S1.4 SNPs and genotype calling in high coverage samples**

Single nucleotide variants and indels were jointly discovered in the 357 autosomal scaffolds belonging to the 13 high coverage individuals using the *UnifiedGenotyper* algorithm implemented in *GATK*. After the individual genotypes calling step, all variants were filtered out if they matched at least one of the following criteria: not a biallelic SNP, a significant fisher strand test (FS<60), a Variant Confidence/Quality by Depth (QD) < 2, a RMS Mapping Quality (MQ) < 40, a MQRankSum < 12.5, a significant read position bias (ReadPosRankSum < -8.0) and an approximate read depth < 20 & > 820. We additionally removed SNPs within 5bp of called indels (reporting a QUAL>30) and SNPs falling in tandem repeated regions according to genome annotations (18). We further filtered each individual excluding genotypes with a coverage <4 and a GQ <30.

The number of SNPs discovered in each high coverage individual across the screened autosomal genome, in the coding part of annotated genes (CDS: ~30Mb) and within regions not containing repetitive elements (tandem repeat regions and transposable elements) and 50kb far from known genes (i.e. the "neutral" partition of the genome - nCDSnREP; ~514Mb) are shown in Table S3. The APN2 individual exhibited the lowest genomic variability among brown bears with ~0.6 heterozygous site every 1000 bp. Segregating sites in all other brown bear individuals were from 2.4 to 3 times more with the exception of the Spanish sample showing 1.7 times more heterozygous sites than the Apennine sample. Interestingly, the polar bear individual showed approximately half of the polymorphic sites as the Apennine one (~0.3 heterozygous site /kb). The same pattern emerged from the analysis of the neutral partition of the genome indicating that demographic events played a fundamental role in shaping the level of genetic variability we observe today. In all brown bears, the level of variation within coding sequences was approximately two times lower than what we observed in the autosomes. In polar bears, we observe only a 16-37% reduction in the amount of polymorphism in the coding regions even though its CDS mean heterozygosity is similar to what we observed in the Apennine brown bear (Table S3).

In order to explore how the genetic variation is distributed along the genome, we estimated the number of segregating sites in 50kb not-overlapping windows using the "--SNPdensity 50000" option in *vcftools* (19) and visualized their frequency distribution using the R package *beanplot* (20). The APN2 individual showed a clear bimodal distribution (Figure S2): the majority of the windows have less than 5 segregating sites (i.e., $\theta_W < 0.0001$) whereas the remaining part  ca. 100. This small portion of the Apennine brown bear genome conserved a level of variation that is comparable to the average genomic diversity in the other brown bear individuals (Figure S3). In the latter, we observed a unimodal frequency distribution centered around 100 segregating sites. Such pattern could be the result of a demographic history characterized by a recent split of the Apennine brown bear from an ancestral brown bear population followed by a strong and persistent decrease in size of the Apennine brown population. The frequency distribution was also bimodal in the Spanish bear individual even if an increased proportion of windows with ca. 100 segregating sites characterized it. In contrast, polar bears showed a clear unimodal distribution around 15-20 segregating sites.

**Table S3. SNPs called in high coverage individuals after filtering**. Only autosomal scaffolds longer than 100kb were used.

| Sample | Autosomes | CDS | nCDSnREP | Het/bp autosomes | Het/bp CDS | Het/bp nCDSnREP |
|---|---|---|---|---|---|---|
| APN2 | 1,247,641 | 9,928 | 309,243 | 0.00058 | 0.00033 | 0.00060 |
| SLK1 | 3,467,893 | 25,977 | 847,033 | 0.00160 | 0.00087 | 0.00165 |
| SPA1 | 2,143,616 | 16,817 | 527,122 | 0.00099 | 0.00056 | 0.00103 |
| ALP1 | 3,856,688 | 29,110 | 915,266 | 0.00178 | 0.00097 | 0.00178 |
| SWE1 | 3,439,608 | 26,837 | 828,040 | 0.00159 | 0.00090 | 0.00161 |
| SWE2 | 3,089,410 | 20,392 | 751,854 | 0.00143 | 0.00068 | 0.00146 |
| POL1 | 660,949 | 6,869 | 151,631 | 0.00031 | 0.00023 | 0.00029 |
| POL2 | 791,634 | 8,668 | 176,583 | 0.00037 | 0.00029 | 0.00034 |
| POL3 | 742,126 | 7,256 | 167,418 | 0.00034 | 0.00024 | 0.00033 |
| POL4 | 792,010 | 8,615 | 177,359 | 0.00037 | 0.00029 | 0.00034 |
| POL5 | 788,338 | 8,655 | 175,306 | 0.00036 | 0.00029 | 0.00034 |
| POL6 | 808,325 | 9,240 | 180,598 | 0.00037 | 0.00031 | 0.00035 |
| BLK1 | 2,536,675 | 21,562 | 598,245 | 0.00117 | 0.00072 | 0.00116 |

**Figure S2: Frequency distribution of the number of segregating sites in high coverage individuals.** Please, note that the constriction from 0 to 0.00002 (corresponding to 0 to 1 segregating sites every 50kb) is a graphical artifact of the plot.

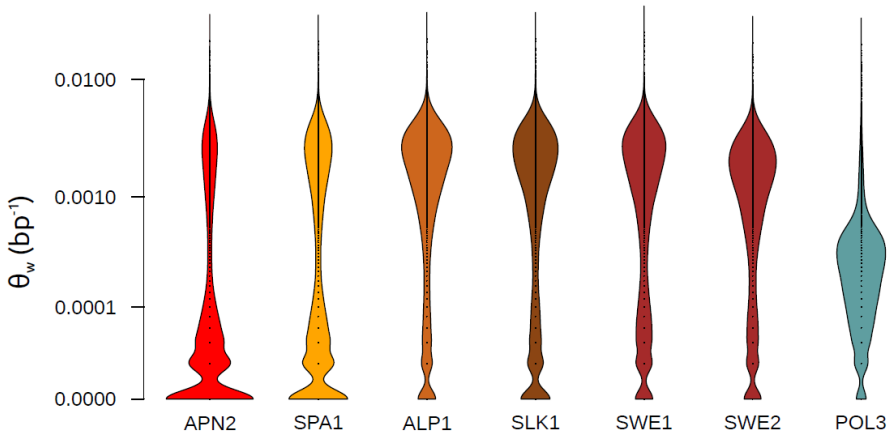

**Figure S3: Estimates of $\theta_w$ across the genome of high coverage individuals**

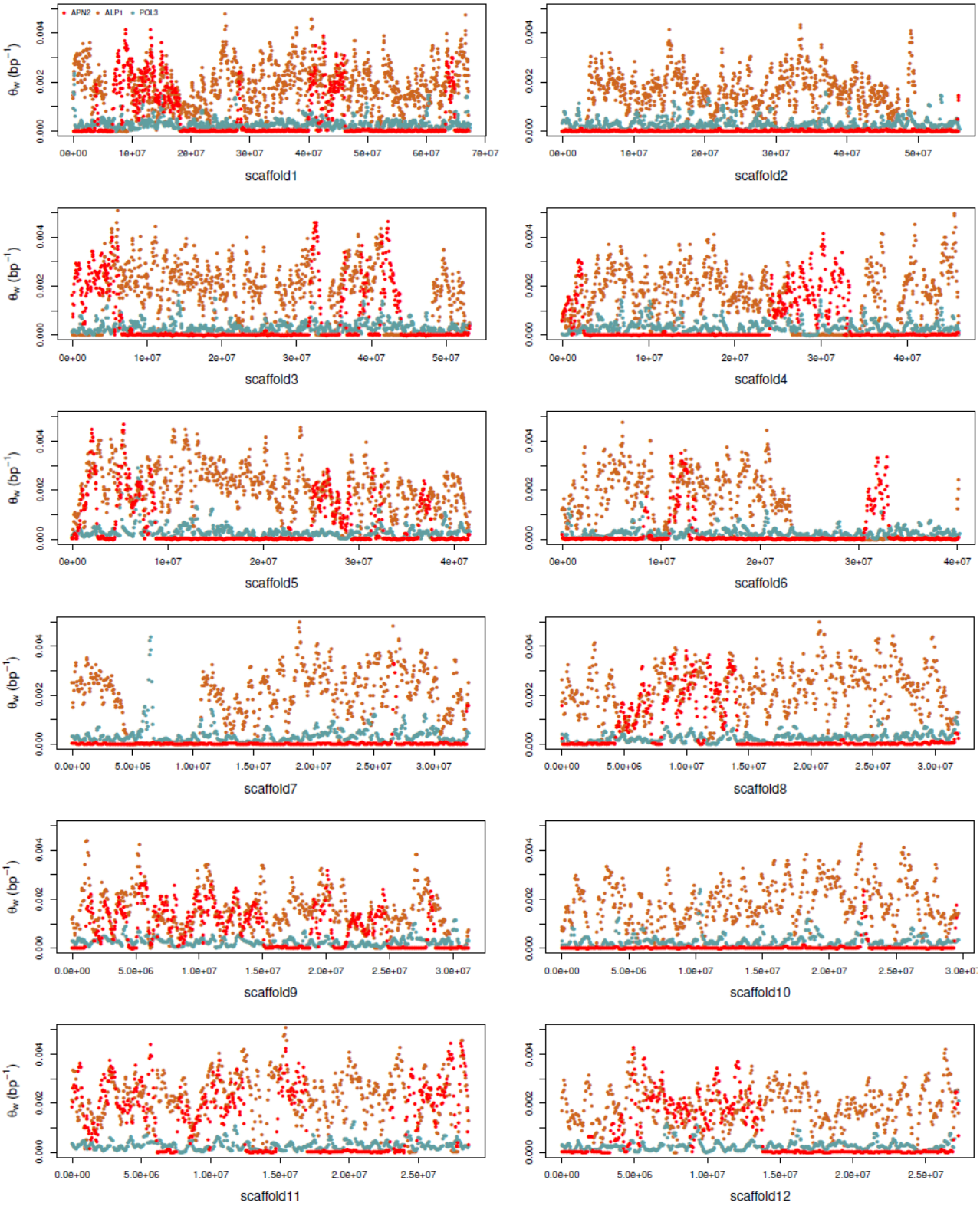

**S1.5 Estimation of $\theta_w$ in low coverage samples**

We used a method implemented in the software *ANGSD* (21) to compute several measure of genetic variation in low coverage samples integrating the genotype uncertainty and dealing with the error rates typical of NGS sequencing. In fact, common genotype callers (e.g. *GATK*) are designed to deal with samples sequenced at high coverage with multiple reads, generally > 15, contributing to the discovery of variants at each genomic position (22). However, when the mean coverage is smaller than 10X, such algorithms exhibit poor performance generally underestimating the number of heterozygous sites and biasing the estimation of parameters related to genetic diversity (23).

The site allele frequency likelihood was initially computed with *ANGSD* using the *GATK* genotype likelihoods model (GL 2) including only reads with a mapping quality >=25 and nucleotides with a base quality score >= 25. Reads marked as not primary, failed or duplicate were also excluded. Based on the computed likelihood, we applied *realSFS* (24) to obtain a maximum likelihood global estimate of the site frequency spectrum over the 357 autosomal scaffolds. To polarize the site frequency spectrum given the ancestral state of each nucleotide position, we generated the consensus sequence of the black bear genome randomly picking one high quality base (mapQ > 25 and baseQ > 25) at each genomic position using the "*-doFasta 1*" option in *ANGSD*. Following the empirical Bayes method introduced in Korneliussen et al (24), we used the maximum likelihood global estimate of the site frequency spectrum as a prior to compute the posterior probability of the allele frequencies at each site. The posterior probabilities were then used to obtain an adjusted site frequency spectrum and to compute different $\theta_w$ (i.e. the population scale parameter $4N_e\mu$ for diploid organisms) estimators for each target genomic region . We used the Watterson estimator of $\theta_w$ (25) calculated in 50kb overlapping windows, with 10kb step, over the 357 autosomal scaffolds, excluding windows with more than 30% of missing sites. $\theta_w$ estimation was performed independently on each of the seven individuals with coverage < 10X and on the 13 high coverage individuals down-sampled to 6X for comparison. The analysis was repeated estimating $\theta_w$ on groups of individuals coming from the same geographical area: Central Italy (APN including APN2, APN3, APN4, APN5, APN6), Greece (GRE1, GRE2), Slovakia (SLK1, SLK2), Sweden (SWE1, SWE2), Central Europe (EUR including GRE1, GRE2, ALP1, SLK1, SLK2), and Greenland (POL including POL1, POL2, POL3, POL4, POL5, POL6). The results for different genomic regions (all autosomes, coding and neutral regions) are reported in Table S4.

**Table S4. Mean $\theta_w$ estimate in low coverage samples using ANGSD**. Samples were analysed individually (n=1) or grouped by geography (n>1). Per site estimates are reported for all autosomes, coding and neutral regions.

| Sample(s) | n | Coverage | $\theta_w$ autosomes | $\theta_w$ CDS | $\theta_w$ nCDSnREP |
|---|---|---|---|---|---|
| APN2 | 1 | 7.65 | 0.00060 | 0.00036 | 0.00058 |
| APN3 | 1 | 5.71 | 0.00070 | 0.00043 | 0.00067 |
| APN4 | 1 | 3.76 | 0.00054 | 0.00033 | 0.00050 |
| APN5 | 1 | 3.22 | 0.00060 | 0.00036 | 0.00057 |
| APN6 | 1 | 6.34 | 0.00063 | 0.00042 | 0.00056 |
| GRE1 | 1 | 4.41 | 0.00232 | 0.00145 | 0.00218 |
| GRE2 | 1 | 6.10 | 0.00180 | 0.00099 | 0.00172 |
| SLK1 | 1 | 5.70 | 0.00155 | 0.00088 | 0.00153 |
| SLK2 | 1 | 5.16 | 0.00158 | 0.00087 | 0.00154 |
| SPA1 | 1 | 6.00 | 0.00096 | 0.00055 | 0.00094 |
| ALP1 | 1 | 6.07 | 0.00168 | 0.00092 | 0.00160 |
| SWE1 | 1 | 5.96 | 0.00136 | 0.00078 | 0.00136 |
| SWE2 | 1 | 6.03 | 0.00175 | 0.00101 | 0.00168 |
| POL1 | 1 | 5.97 | 0.00026 | 0.00019 | 0.00024 |
| POL2 | 1 | 5.89 | 0.00024 | 0.00019 | 0.00022 |
| POL3 | 1 | 6.01 | 0.00025 | 0.00018 | 0.00023 |
| POL4 | 1 | 5.86 | 0.00024 | 0.00021 | 0.00022 |
| POL5 | 1 | 5.92 | 0.00025 | 0.00021 | 0.00022 |
| POL6 | 1 | 6.10 | 0.00026 | 0.00021 | 0.00023 |
| BLK1 | 1 | 6.01 | 0.00094 | 0.00065 | 0.00089 |
| SLK | 2 | 10.86 | 0.00162 | 0.00089 | 0.00158 |
| SWE | 2 | 11.99 | 0.00170 | 0.00093 | 0.00169 |
| GRE | 2 | 10.51 | 0.00188 | 0.00108 | 0.00180 |
| POL | 6 | 35.75 | 0.00033 | 0.00025 | 0.00028 |
| APN | 5 | 26.68 | 0.00053 | 0.00032 | 0.00048 |
| EUR | 5 | 27.44 | 0.00195 | 0.00109 | 0.00186 |

**S1.6 Long regions of homozygosity**

In order to quantify the proportion of the genome characterized by long regions of homozygosity in each individual, we computed per site observed heterozygosity in not-overlapping 50kb windows in five high coverage brown bear individuals (APN2, SLK1, SPA1, ALP1, SWE1) using the called genotypes. As short scaffolds could prevent the identification of long homozygous regions and potentially bias the length distribution toward shorter fragments, we restricted the analysis to the 13 longest scaffolds (from 26 to 67 Mb), including 513Mb in total (approximately ¼ of the bear genome). The heterozygosity profile along the scaffolds was then explored to identify long regions (>=1Mb) composed by contiguous windows with less than 25 segregating sites. Such regions have therefore a heterozygosity value constantly lower than 0.0005.

Approximately 75% of the APN2 genome analyzed is composed by long regions of homozygosity with nearly zero variation between chromosomes suggesting a strong effect of genetic drift and inbreeding on this isolated population (Fig. 1D in the main text). Other brown bear individuals from Alps, Slovakia and Sweden show between 13% and 20% of the genome characterized by regions of homozygosity whereas the proportion increases to ca. 50% in the individual from Spain compatible with the history of isolation of this population. Notably, the length of the homozygosity regions peaked to 50Mb in the APN2 sample whereas only to less than 30Mb in the SPA1 sample. In the other brown bear samples, the maximum length is always below 20 Mb (Fig. 1D in the main text).

**S2 Inbreeding estimates**

Average heterozygosity estimates were initially obtained by calculating values of $\theta_w$ estimator for each individual genome (i.e. high and low coverage samples) in 50 kb sliding windows overlapping with a step size of 10 kb. Windows with more than 5,000 missing sites were discarded. To account for differences in mean sequencing depth across genomes, we randomly sampled individual sites in order to match the lowest mean depth reported using SAMtools (26). To further account for data uncertainty associated with low and variable sequencing depth, values were estimated using a probabilistic framework based on genotype likelihoods (21, 24).

To quantify and compare the level of inbreeding across all individuals, we adopted a methodology presented elsewhere (27). This approach uses the proportion of genome segments that are mostly homozygous as a proxy for the inbreeding coverage level. We used a previously implemented pipeline (28, 29) to identify tracts with a unique heterozygosity estimate corresponding to the mean TW, in log scale, for the windows covered. We used the heterozygosity values in windows estimated as explained above. We allowed up to 12 change points during the binary segmentation algorithm for each chromosome. The length of such tracts was calculated from their external coordinates and a density was fitted to their associated TW values using the tract lengths as weights. The rationale of this method is that a distribution of heterozygosity values normalized by segment length appearing bimodal indicates levels of inbreeding, while a unimodal distribution suggests low, if any, inbreeding levels. The minimum point between the two modes was numerically calculated. This value represents a threshold for calculating the fraction of the genome with homozygous tracts;the inbreeding coverage was then estimated by summing the density below the threshold followed by normalization. Further details can be retrieved in the original implementation of such method (28, 29). The inbreeding coverage estimated has been shown to be proportional to the inbreeding value calculated from pedigree (30).

Apennine brown bear individuals (APN2-6) have the highest inbreeding coverage spanning 0.70 to 0.77; the remaining brown bears exhibit lower values of inbreeding, ca. 0.25, with the exception of the sample from Spain, which shows an inbreeding coverage of 0.57 (Fig. S4). To assess whether our downsampling process

affected such values, we repeated the above procedure using the subset of high sequencing depth samples only (Fig. S5). We obtained very similar results to what retrieved using low sequencing depth data, corroborating our findings of lower heterozygosity and higher inbreeding in Apennine samples compared to other brown bears.

**Figure S4. Frequency distribution of heterozygosity estimates for genomic tracks, weighted by length, in low coverage and downsampled high coverage data.** Bimodal distributions are indicative of inbreeding. Values of the inbreeding coverage, and index of inbreeding correlated to the inbreeding coefficient, are reported for each individual. Inferred density plots of the average heterozygosity, in log scale and windows, are reported. The vertical red line denotes the position of the minimum point between the two modes. The estimated inbreeding coverage is shown next to the red line.

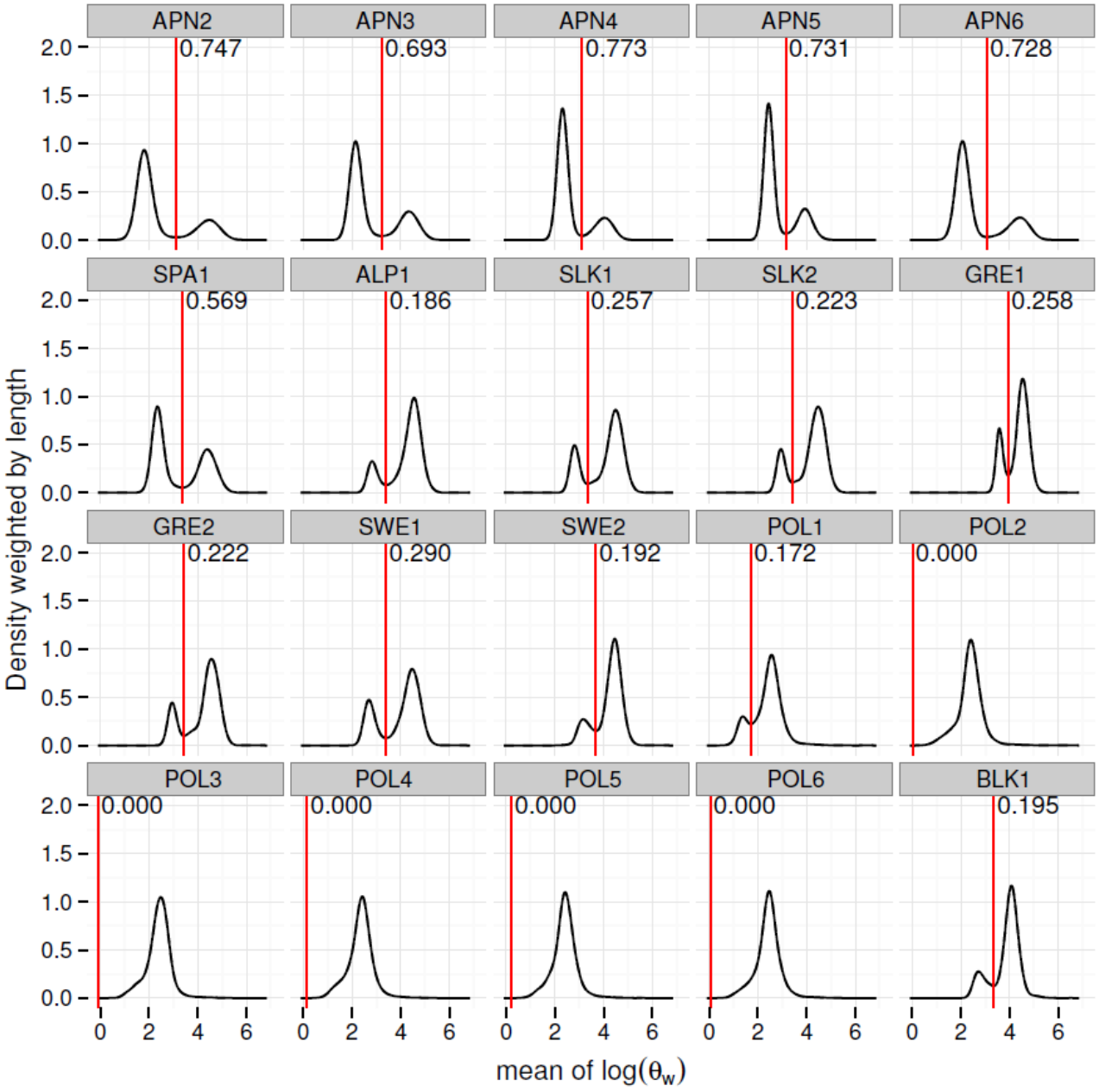

**Figure S5. Frequency distribution of heterozygosity estimates for genomic tracks, weighted by length, in high coverage data.** Bimodal distributions are indicative of inbreeding. Values of the inbreeding coverage, and index of inbreeding correlated to the inbreeding coefficient, are reported for each individual. Inferred density plots of the average heterozygosity, in log scale and windows, are reported. The vertical red line denotes the position of the minimum point between the two modes. The estimated inbreeding coverage is shown next to the red line.

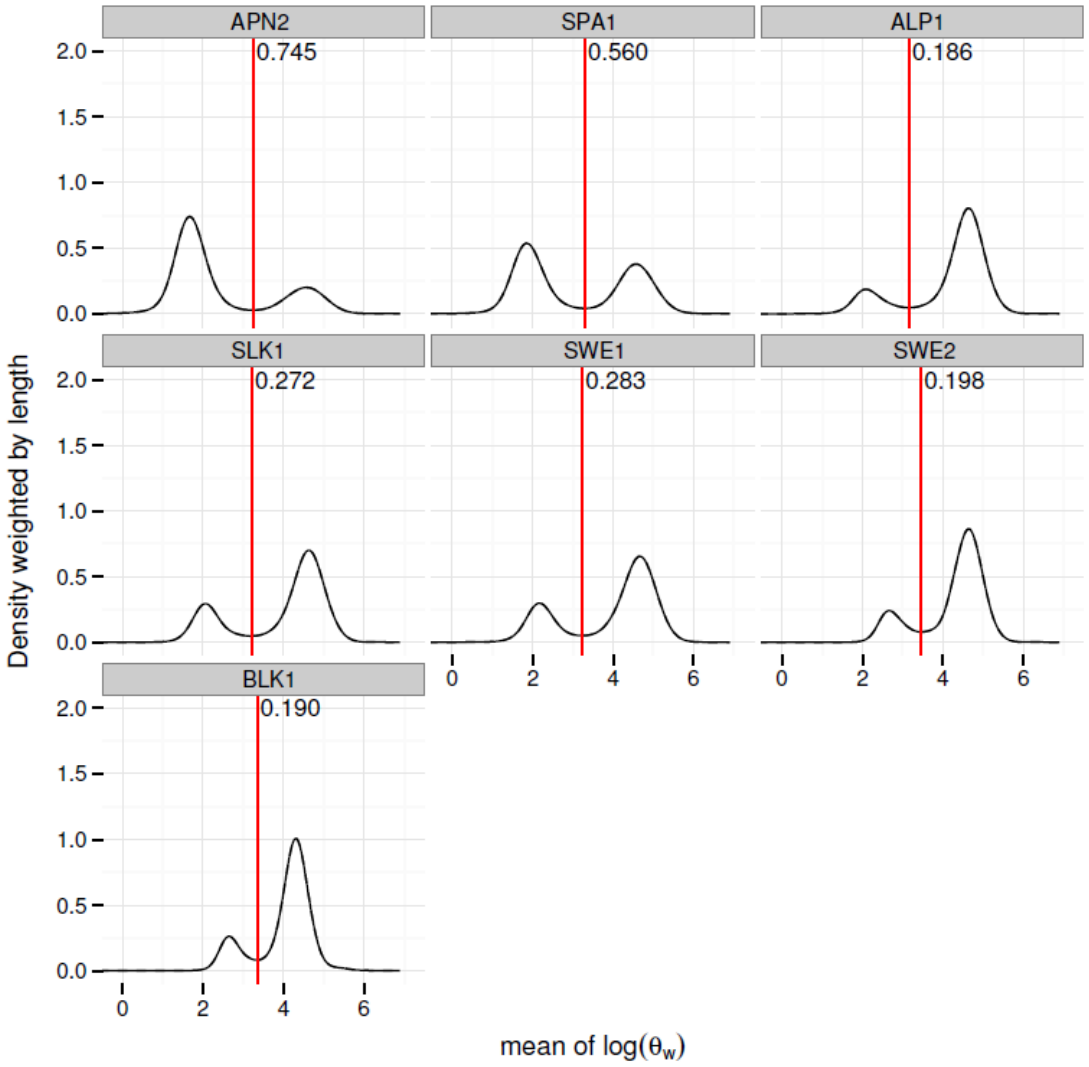

## S3 Demographic analyses

### S3.1 Pairwise Sequential Markovian Coalescent (PSMC) reconstructions

In order to study the past population size variation through time, we applied the PSMC method (31) to the high coverage brown bear samples from our study and we estimated the demographic history in two published brown bear genomes from Sweden for comparison (Fig. S6). The diploid consensus sequence for each sample was called using the Samtools *mpileup* command setting the "-C50" option in order to penalize reads with multiple mismatches reducing their mapping quality. Only genomic positions with a coverage included between 1/3 and twice the average were used, and nucleotides with a base quality score <20 were marked as missing data. The consensus sequence was then transformed in the required format using the *fq2psmcfa* tool (bundled in the PSMC package) and analysed with the *PSMC* model using the following command: *psmc -N25 -t15 -r5 -p "4+25*2+4+6" -o result.psmc diploid_consensus.psmcfa.*

Estimated parameters were scaled in order to have time expressed in years and effective size in number of diploid individuals, using a mutation rate of $1.82*10^{-8}$ per site per generation (11) and a generation time of 11 years. The uncertainty around the estimate was evaluated by bootstrap, splitting genomic scaffolds into smaller segments with the *splitfa* utility and replicating the PSMC analysis on 100 dataset generated by randomly sampling with replacement from the segments pool (activating the "-b" option in PSMC).

**Figure S6**. **PSMC demographic reconstruction inferred using high coverage data from five geographic areas in Europe**. Median is reported as a solid line in the main figure. Bootstrap confidence regions are reported as shaded areas in separated inset figures for clarity.

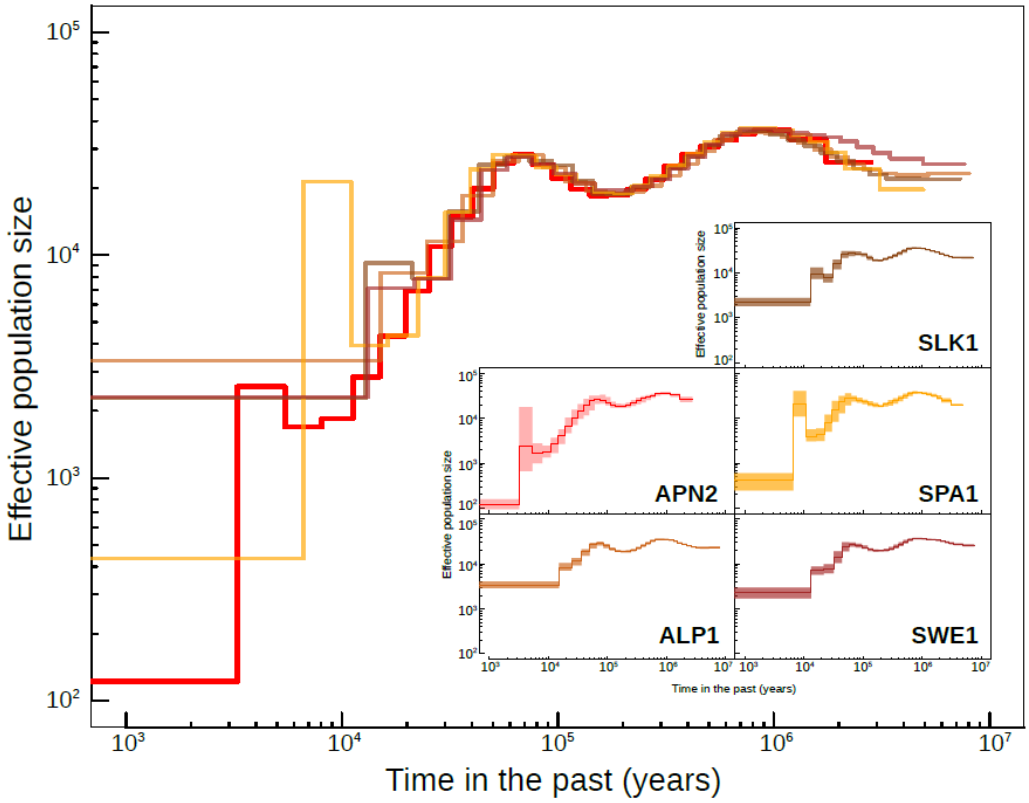

**S3.2 Approximate Bayesian Computation and ABC-Skyline reconstruction**

The demographic dynamic of the Apennine brown bear population was estimated by Approximate Bayesian Computation using the genomic data from the five Apennine individuals in our data set. We developed an approximate Bayesian computation framework (32, 33) to estimate changes of the effective population size through time (ABC-skyline, (34)). An analogous approach has been recently implemented on whole genome data and it was shown to outperform PSMC and related methods under several simulated scenarios (35). Similarly to PSMC, (35) fixed the time points when $N_e$ is allowed to change. Here, we relaxed this assumption by co-estimating $N_e$ and the time points. ABC-skyline can be used on any sample size, so we could include the five Apennine brown bear genomes, from which we selected 4668 independent loci of 4000 bp in length each from non coding regions. To model the evolution of the Apennine brown bear population, we simulated three demographic scenarios with one, two, or three population size changes. The simplest model (Fig. S7) obtained the highest posterior probability and we therefore used this model to estimate three parameters: modern $N_e$ ($N_{mod}$), ancestral $N_e$ ($N_{iso}$) and the time of change ($T_c$). We also recorded the *Resize* parameter, which is the $N_{iso}$/ $N_{mod}$ ratio: values lower than 1 implies population expansion, values higher than 1 implies population contraction.

**Figure S7. Demographic model used for the ABC-Skyline inference**

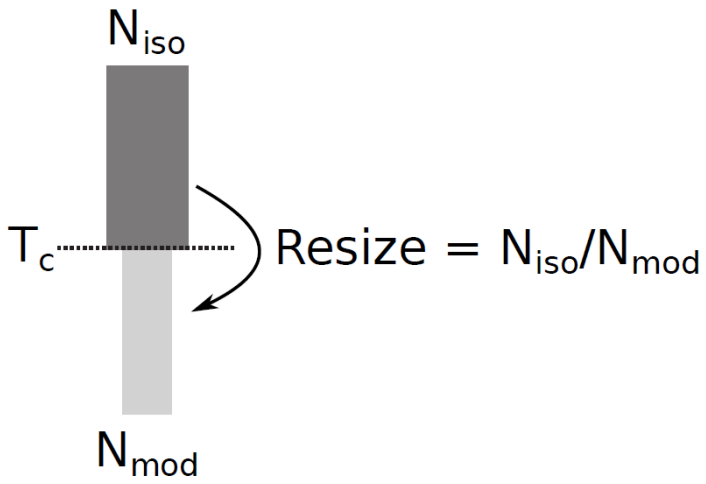


We generated 100,000 simulations for each demographic model using fastsimcoal2 v2.5.1 (36). Each simulation includes 4668 independent gene genealogies corresponding to the above selected unlinked loci. We let mutation and intra-locus recombination rates vary across loci by setting a normal hyperprior distribution on both of them. The mean of the hyperprior distribution of the mutation and recombination rate was modelled as uniform between 1.5 and 2 x $10^{-8}$ and between 0 and $10^{-8}$ per site per generation, respectively. For the standard deviation on both hyperprior distributions, a uniform distribution between $10^{-11}$ and $10^{-10}$ was applied. With such hyperprior distribution on both mutation and recombination rates, we could take into account variation in both mutation and recombination rates across the genome. Moreover, by modelling intra-locus recombination we could use multiple SNPs coming from the same region. Posterior estimates for the demographic parameters with the associated prior distributions are shown in Figure S8 and Table S5. The unfolded site frequency spectrum was used as summary statistics. Parameters of each model were estimated using a nonlinear regression (37) on the 5,000 simulations producing an SFS closest to the observed data. The non-linear regression has been recently shown to

perform better than the classic Beaumont local linear regression under demographic scenarios similar to those implemented here (35).

For each combination of parameters retained by the ABC algorithm (5,000 in our case), we recorded the effective size at specific time points. The median value of the posterior distribution of the effective size at each time point was calculated together with the 95% credible interval and plotted against time to obtain an ABC-skyline reconstruction (Fig. 2 in main text). Time points were defined by randomly extracting 300 values from an exponential distribution with a rate calibrated up to 200,000 generations ago. Moreover, additional time points (25, 50, 100, 200, 300, 400, 500, 600, 700, 800, 900, 1000, 1500, 2000, 2500, 3000) were manually added to increase the resolution towards recent events. Analyses were performed in the R environment with the library *abc* (38). To test the validity of our method, we applied the same framework to 1,000 pseudo observed datasets (*pods*) simulated with a constant Ne=5,000 and the same number of loci, mutation rate and intra-locus recombination rate.

**Figure S8**. **Posterior distributions of the demographic parameters estimated in the Apennine brown bear population using the ABC-Skyline approach.** Prior distribution for each parameter is reported as dashed black line.

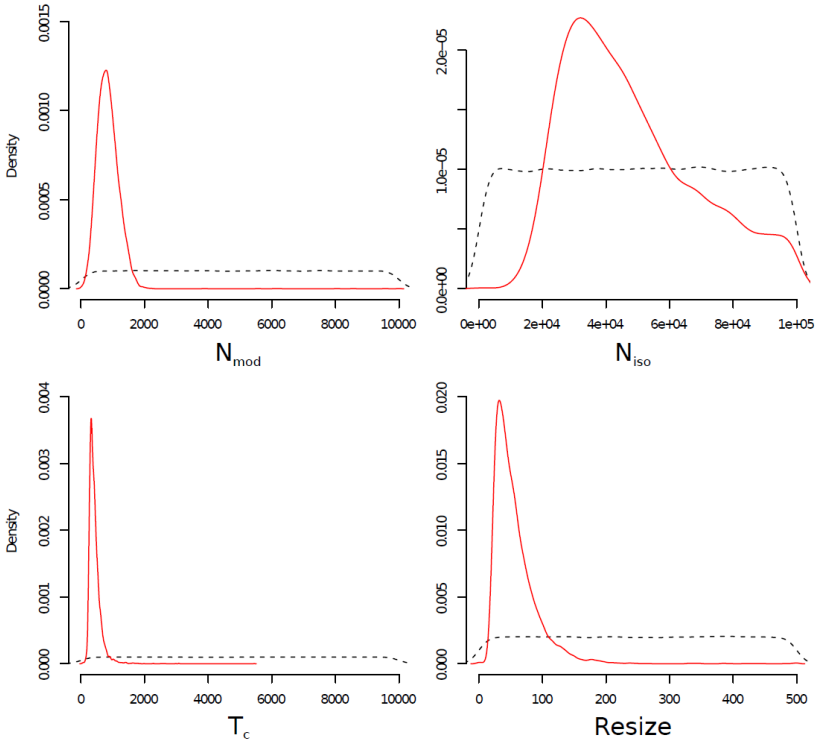

**Table S5. Estimated demographic parameters in the Apennine brown bear population using the ABC approach.** [a]Upper and lower limits of the 95% credible interval of the posterior distribution. [b]U:uniform probability, in the range of the two values. Time is in years, assuming a generation time of 11 years.

| | Median | Mode | 0.025[a] | 0.975[a] | Prior[b] |
|---|---|---|---|---|---|
| $N_{mod}$ | 855 | 828 | 324 | 1552 | U:10-10,000 |
| $N_{anc}$ | 43,224 | 31,467 | 20,143 | 95,321 | U: 10-100,000 |
| **Resize** | 43.9 | 30.7 | 20.9 | 134.4 | |
| $T_c$ | 4444 | 3663 | 2541 | 8790 | U:10-10,000 (in generations) |

**S3.3 Comparing patterns of homozygosity regions in real and simulated genomes**

In order to identify the strength of the population contraction that could have produced the accumulation of homozygosity regions in the Apennine brown individuals, we performed coalescent simulations with ms (39) to model the expected patterns of homozygosity regions (PHR) in the genome under different demographic conditions. Two chromosomes of 50Mb in length were simulated under an instantaneous population decline model reducing the ancient population size (*NA*) to what we observe in the present (*N0*), *T* generations in the past. We analysed three possible *NA* (10000, 20000 and 40000 diploid individuals), *N0* (20, 50, and 100 diploid individuals) and *T* (50, 100 and 300 generations), defining a grid of 27 parameter combinations. Variation along the chromosomes were introduced using an infinite mutation model with a mutation rate of $1.82^{-8}$ per site per generation (11) and a mammalian recombination rate of $1^{-8}$ per site per generation (40). Twenty simulations were performed for each parameter combination and in each simulation, heterozygosity was computed in 50kb not-overlapping windows detecting contiguous segments of nearly zero variation (obs. Het. < 0.0005). We first compared the observed proportion of homozygosity regions in the Apennine brown high coverage individual (see S1.6) with the simulations for each parameter combination (Fig. S9). For several parameters combinations, the observed value was included in the simulated values space: e.g. i) extremely low modern population sizes (N0=20,50) in combination with the most recent reduction time (T=50), or ii)moderately small population size (N0=100) and ancient time of the decline (T=300). As the simple proportion of homozygosity might not take into account all the features describing how $\theta_w$ is distributed along two chromosomes, we plotted the (absolute) frequency distribution of $\theta_w$ values (window-wise) computed in the observed and simulated data (Fig. S10). A clear match between the two profiles would support the suitability of the simulation parameters.

A visual inspection of the overlap indicated that most of the parameter combinations produced clearly different $\theta_w$ distribution than the observed one, especially for high $\theta_w$. The best fitting scenario is characterized by a bottleneck occurred 300 generations in the past, from an ancestral population size of 40,000 to a modern size of 100 individuals (Fig. S10). From this set of parameters, we separately doubled each value (last row of plots in Fig. S10) and verified a clear worsening of the fit. We analysed the robustness of our results with respect to the recombination rate (10 times slower) and sequence length (10 times higher). No significant deviations were observed for a ten times slower recombination rate and a ten times longer sequence.

**Figure S9. Fraction of homozygosity regions in demographic simulations and in the Apennine brown bear high coverage genome**. The proportion of long homozygous regions in a 50Mb diploid genome is computed in 20 coalescent simulations under different demographic conditions. The observed value in the high coverage Apennine brown individual (0.75) is represented by a red horizontal dashed line. N0: present population size, NA: ancient population size, T: time to the bottleneck in generations.

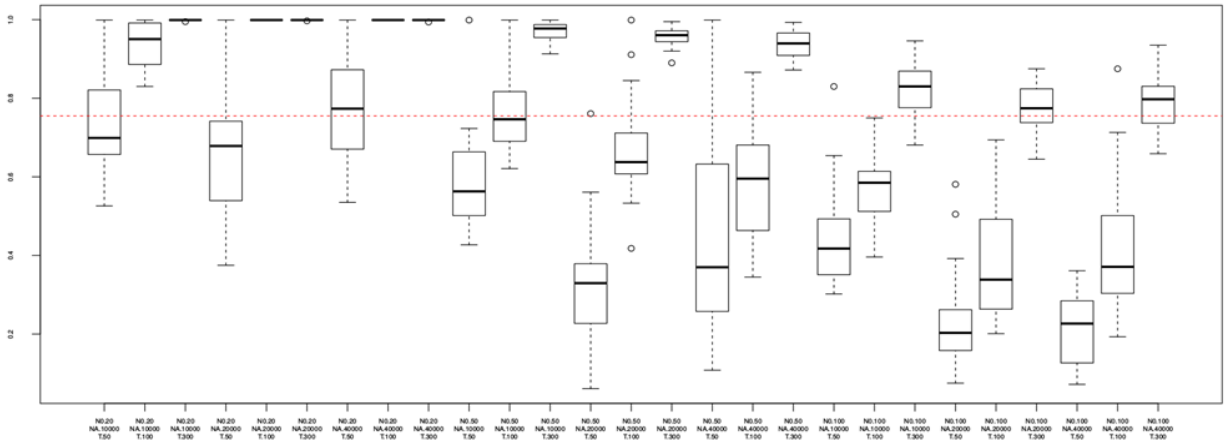

**Figure S10**. **Pattern of $\theta_w$ in demographic simulations and in the Apennine brown bear high coverage genome.** Values of $\theta_w$ (in ascending order; red lines) per window, computed in 1000 windows of 50kb in 20 simulations per each demographic scenario (i.e. different bottleneck parameters). The black line represents the $\theta_w$ distribution in the observed high coverage Apennine brown genome. N0 and NA correspond to the modern and the ancient population size, respectively, whereas T is the age of the bottleneck in generations. The best fitting scenario in indicated with a black box.

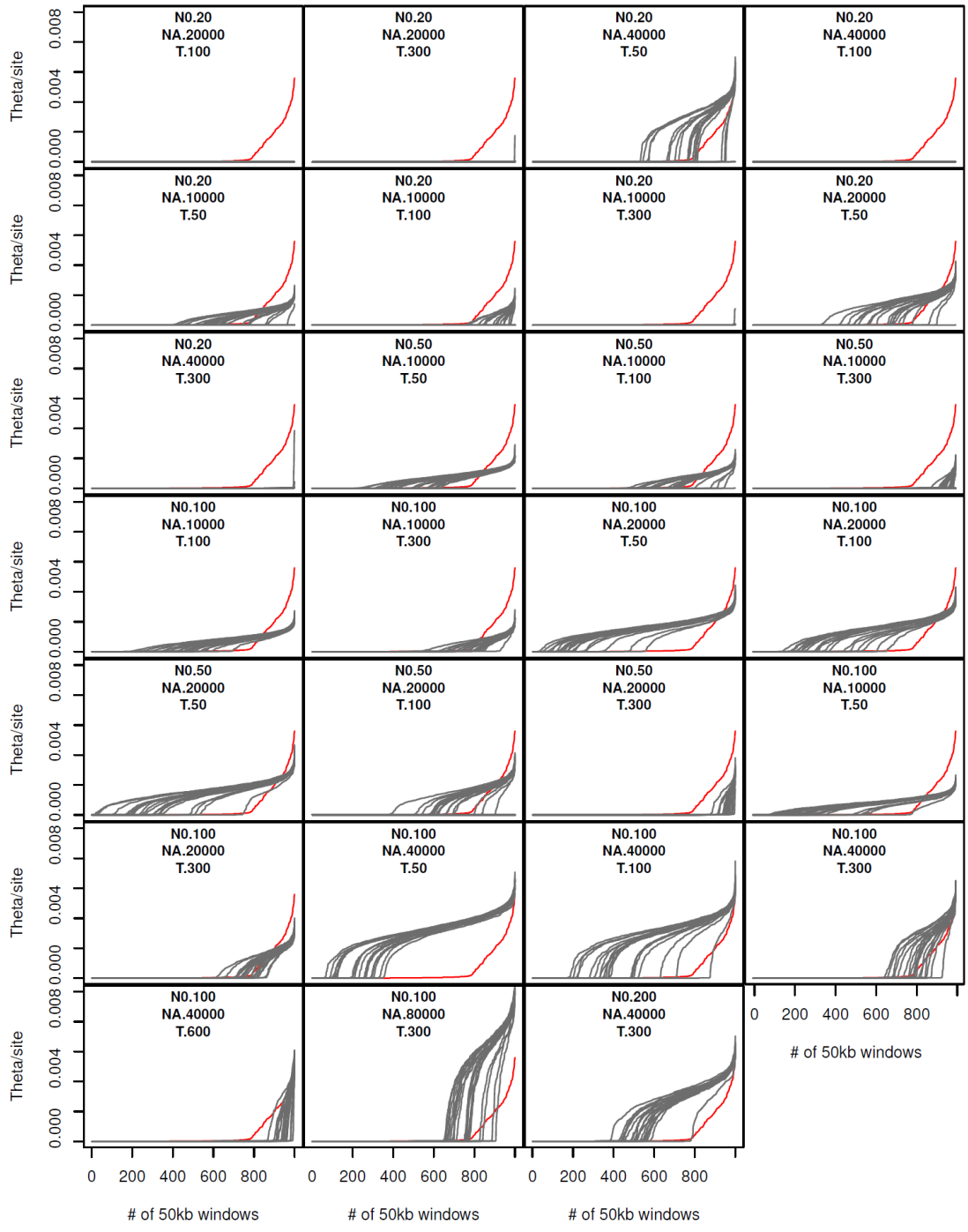

### S4 Neighbor-Joining tree on whole-genome distances

We used ANGSD to compute pairwise genomic distances between individuals without calling genotypes. The low coverage alignments from five Apennine brown, eight European Brown, six Polar and one Black individuals were included in the analysis applying the same quality filtering described above in the $\theta_w$ estimation in the low coverage samples" section. Firstly, for each genomic position, we identified the major and minor allele using the approach proposed in Skotte et al 2012 based on the GATK genotype likelihoods (GL 2) assuming that each site could be biallelic only ("-doMajorMinor 1"). This information was then used to compute the genotype posterior probabilities for each of the three possible genotypes (major,major; major,minor; minor,minor) at each locus setting the "-doGeno 8" option and using the estimated allele frequency as a prior ("-doMaf 1"). We included in the analysis only genomic positions from the 357 autosomal scaffolds and covered by reads in all 20 individuals. The posterior probabilities were then used in *ngsDist* (11, 41) to obtain the pairwise distance matrix between individuals for each scaffold. Since all distances are restricted to be in the [0,1] interval and longer scaffolds contain more information than small ones, we weighted each one of the 357 distance matrices by the scaffold length, thus obtaining a unique matrix computed over 1,842,042,551bp. The neighbor joining tree based on such distance matrix was computed using the R (R core team 2013) function *nj* from the *ape* package (42). The neighbor-joining tree on whole-genome distances is shown in Figure 1 in the main text.

## S5 Population structure analysis

### S5.1 Groups inference with STRUCTURE

We inferred the individual-based genetic structure using the Bayesian population model implemented in STRUCTURE 2.3.4 (43, 44). The STRUCTURE algorithm allows to identify clusters of related individuals from multilocus genotyping data assigning to each individual a membership probability to each of a specified number of ancestral groups (K). We ran this analysis considering all low coverage brown and Apennine brown bear individuals (13 in total). We included only SNPs at least 50 kb far from any known gene and not in repeated regions.

We initially explored the pattern of LD decay along scaffolds longer than 1Mbp in five Marsican and five European individuals, respectively. To take into account data uncertainty due to low-coverage samples, we inferred LD values from genotype likelihoods estimated with ANGSD (https://github.com/fgvieira/ngsLD). Specifically, we calculated $r^2$ using an EM algorithm to estimate haplotype frequencies between each pair of SNPs (adapted from bcftools v0.1.18 (15)). We randomly sampled five million pairs and calculated the average $r^2$ in windows of 1kbp. LD decays to its expected value, which depends on the sample size, in the first few thousand base pairs in the European samples. The decay is slower in the Marsican group, as expected when the population size is low (Fig. S11). Such background LD due to drift within the Marsican population is not expected to produce any bias in our Structure analysis. In fact, background LD tends to artificially increase the number of genetic components, and this bias, which occurs more frequently when small population, isolated since long time, come together producing an excess of admixture LD, can be usually detected when most (all) individuals in different populations are admixed (44). None of this is observed or inferred in our Structure analysis (see below).

We then filtered for linkage disequilibrium considering SNPs separated by at least 150 kb according to the LD decay in the European individuals. The final dataset consisted of 7,971 unlinked polymorphic loci. We ran 10 independent runs of STRUCTURE, each with 100,000 burn-in iterations and 300,000 MCMC iterations for K values ranging from 2 to 5, under the admixture ancestry model and with no location prior.

We monitored alpha and likelihood values to assess the convergence during burn-in and MCMC iterations. The output from STRUCTURE was analyzed in STRUCTURE HARVESTER (45), which implements the Evanno method (46) to infer the most likely number of differentiated populations. Replicate runs for each K were averaged in CLUMPP (47) using the Greedy algorithm and 10 random input sequences. Results in Figure S12.

To decisevely exclude that background LD in the Apennine bear population introduced a bias in the STRUCTURE analysis, we performed additional Structure analyses selecting one SNP approximately every 70 SNPs in the list of ordered 7,971 SNPs obtained randomly joining the scaffolds. The map distance between the SNPs in the reduced data set is not known (scaffold are not assembled into chromosomes) but at least for SNPs on the same scaffold this distance is larger than 10 Mb (150kb x 70). We replicated the STRUCTURE analysis testing K ranging from 2 to 6 in 10 replicated run implementing 50,000 burn-in iterations and 100,000 MCMC iterations. Results fully support the large divergence of the single Apennine component and the absence of shared components between the Apennine bears and the the other groups. (Fig. S13).

**Figure S11. Linkage disequilibrium decay.** Average $r^2$ in windows of 1kbp estimated on 5 million random pairs of SNPs from scaffolds longer than 1Mbp in five European (A) and five Marsican (B) individuals. SNPs separated by at least 150kbp (solid vertical line) were used in the main STRUCTURE analyses.

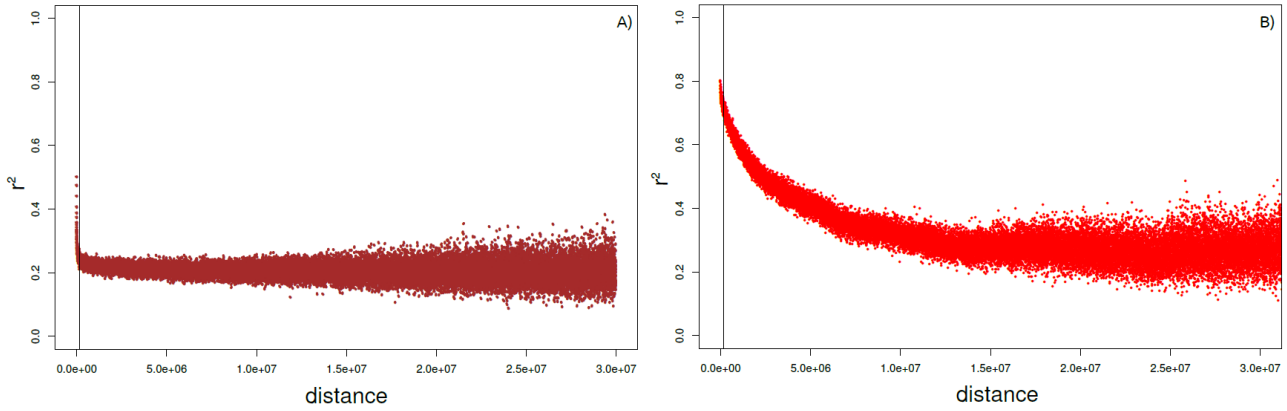

**Figure S12. Genomic components of single individuals (STRUCTURE analysis)**. The analysis is based on 7,971 SNPs in non-coding and non-repetitive regions, separated by at least 150kb. K is increasing from 2 to 5, with 5 being the most likely number of groups. Apennine brown bear individuals always cluster together as a distinct genomic group; Greece, Slovakia, Sweden, and Spain emerge as four additional groups; the Slovenian/Alpine individual shows a mixed ancestry where the Apennine brown component is present but negligible.

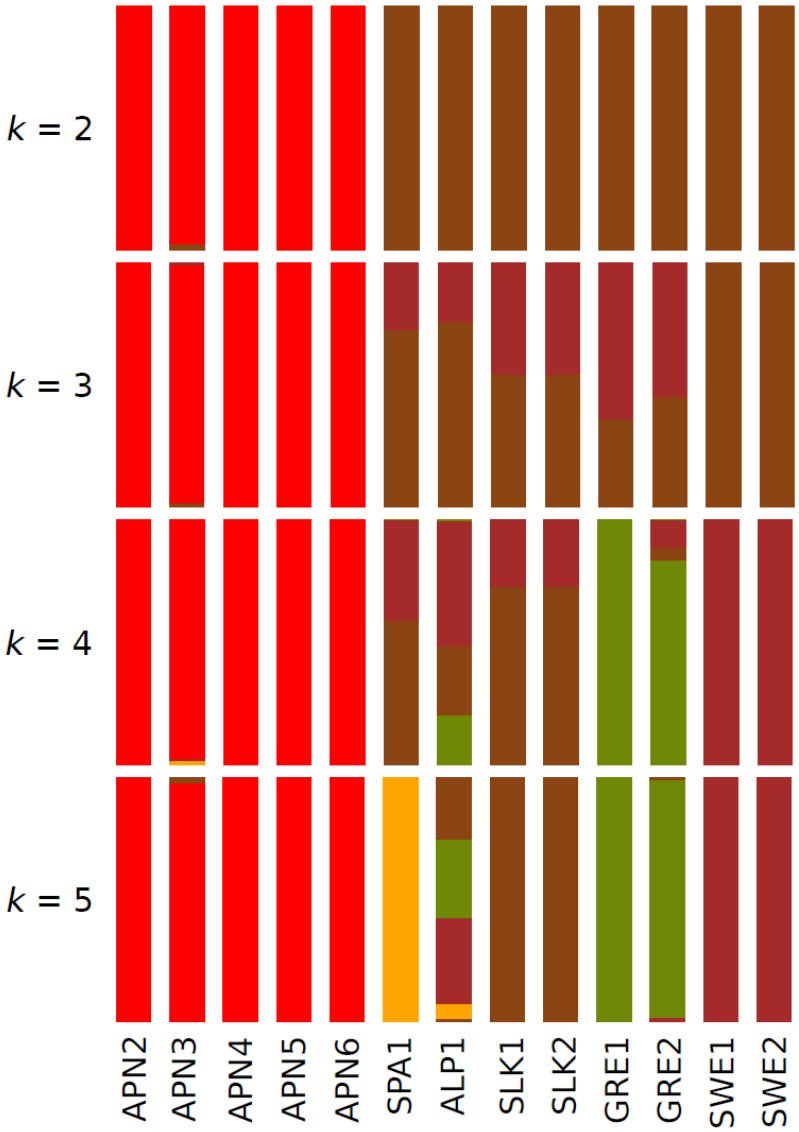

**Figure S13. Validation of STRUCTURE analysis in Fig. S12.** The analysis is based on 100 SNPs in non-coding and non-repetitive regions, separated by at least 10Mb when on the same scaffold.

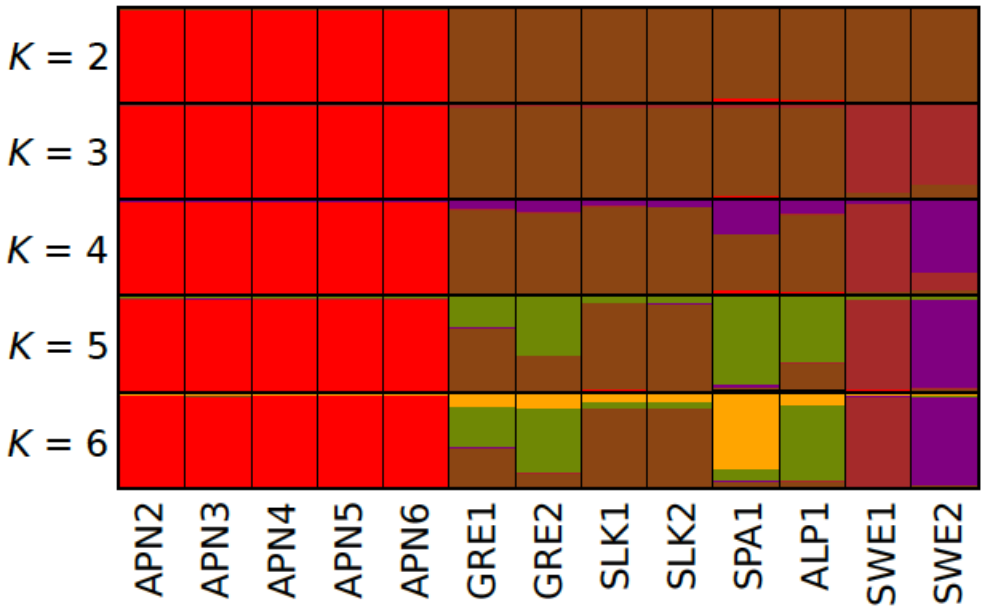

**S5.2 Meta-population modelling with ABC**

Populations rarely evolve as isolated entities but they rather belong to networks of demes exchanging migrants to some extent. Many recent works have shown that failing to take the structure of the metapopulation into account may lead to spurious signatures of effective population size changes through time (48, 49) or leave a genetic footprint similar to episodes of ancient hybridization (50). Moreover, species are likely to go through complex histories and it may be challenging to distinguish between local events (such as a bottleneck or expansion in a deme) and changes in connectivity among demes of a metapopulation (51). Indeed, a bottleneck detected using a model in which structure it is not accounted for (such as the PSMC or the ABC-skyline; see above) may be due to either the local reduction of population size, or a reduction of migration rate between this deme and the others, or both (51). To further explore the evolutionary history of the Apennine brown bear population we therefore build a complex metapopulation model (model FIM, (34)) relating all European populations (Fig. S13).

**Figure S14. The ABC metapopulation model.**

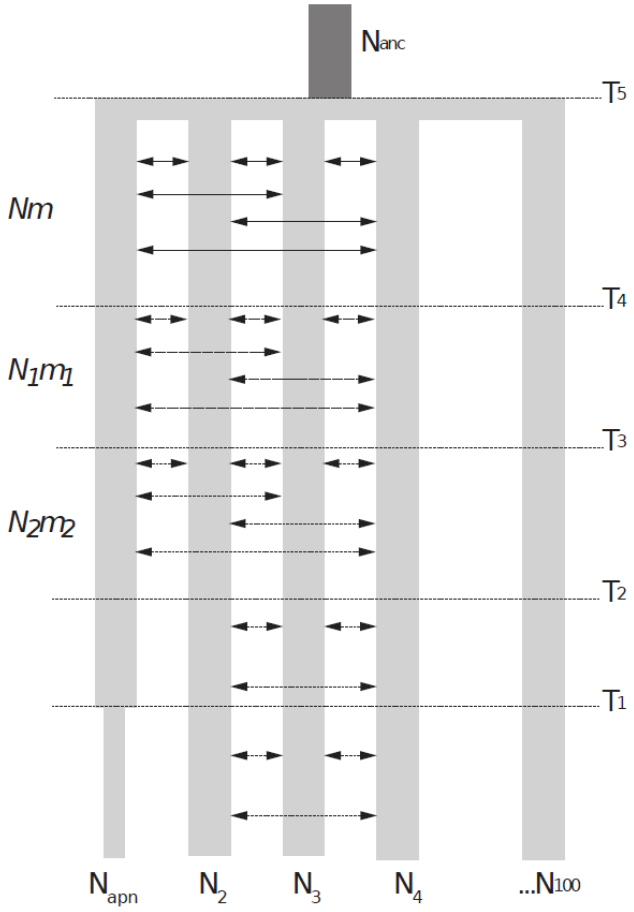


We devised the metapopulation model starting from our preliminary results as well as previous evidences: i) the Apennine brown bear population is almost equally isolated from all European populations (based on nuclear data); ii) there is no clear geographical pattern in Europe (i.e., all populations appears to be equally distant from each other, not only when compared against the Apennine one); iii) Apennine population experienced a recent decrease in Ne according to our unstructured demographic models (PSMC and ABC-

skyline). We followed an ABC approach as explained in the ABC-skyline section (see above) in terms of number of loci, mutation and recombination rate, number of simulations and the ABC algorithm for parameter estimation. Here, the dataset is made of the five Apennine individuals (corresponding to one deme) and four European individuals (corresponding to 4 independent demes): one from the Alps (ALP1), one from Sweden (SWE2), one from Slovenia (SLK1) and one from Greece (GRE2). As summary statistics we chose the unfolded site frequency spectrum of the Apennine population and the average 2D site frequency spectrum across the four European samples. We simulated a non-equilibrium 100 demes finite island model with the following characteristics: looking forward in time, an ancestral deme (with its own effective size $N_{anc}$) gives rise to the 100 demes at $T_5$ generations ago. Since then, all demes exchange migrants under a symmetric migration matrix defined by the compound parameter $Nm$. Here, N represents the size of each deme and $m$/99 the migration rate to any of the other demes. $Nm$ is therefore the total number of migrants going out from a deme each generation backward in time. At time $T_4$ a change of connectivity is modeled, with the migration matrix characterized by the new $N_1m_1$ parameter. A new change in the matrix is simulated at $T_3$ generations, and demes continue exchange migrants at a $N_2m_2$ rate until present. At $T_2$, the deme corresponding to the Apennine population stops exchanging migrants with all the others, becoming isolated. Finally, at $T_1$ the Apennine deme ($N_{apn}$) experiences a reduction of its effective size. Posterior distributions and estimates of the demographic parameters, and their prior distributions, are provided in Figure 3 in main text and Table S6. Finally, a posterior predictive test (52) was carried out to test whether the data can be reproduced under our specific demographic model. We simulated 10,000 pseudo-observed datasets (pods) by randomly extracting parameters from the ABC posterior distributions. For each pod, the nucleotide diversity and total number of segregating site were calculated and then plotted against the real value. For each pod, the nucleotide diversity and total number of segregating site were calculated and then plotted against the real value.

**Table S6. Estimated parameters in the ABC meta-population model.** $N_{apn}$: effective population size of the modern Apennine population; $N_{anc}$: ancestral effective population size (founding deme of the metapopulation); $T_1$, $T_2$, $T_3$ and $T_4$: time of the demographic change (in generations); $T_5$: time of the onset of the metapopulation (in generations); $Nm$, $N_1m_1$ and $N_2m_2$: product of the effective population size $N$, $N_1$ and $N_2$ and the migration rate $m$, $m_1$ and $m_2$ for each deme. [a]Upper and lower limits of the 95% credible interval of the posterior distribution. [b]U, uniform probability, in the range of the two values.

| Model FIM | Median | Mode | 0.025[a] | 0.975[a] | Prior[b] |
|---|---|---|---|---|---|
| $N_{apn}$ | 281 | 174 | 43 | 846 | U:10-1000 |
| $N_{anc}$ | 50,630 | 53,700 | 26,762 | 76,332 | U:100-100,000 |
| $T_1$ | 76 | 22 | 3 | 517 | U:1-$T_3$ |
| $T_2$ | 165 | 73 | 20 | 1003 | U:$T_1$-$T_3$ |
| $T_3$ | 320 | 165 | 51 | 1664 | U:1-2,000 |
| $T_4$ | 4908 | 2282 | 973 | 9790 | U:$T_3$-10,000 |
| $T_5$ | 23,726 | 14,084 | 6910 | 90,037 | U:$T_4$-100,000 |
| $Nm$ | 115.66 | 57.03 | 26.84 | 484.57 | U:0.5-500 |
| $N_1m_1$ | 188.73 | 65.43 | 14.41 | 485.10 | U:0.5-500 |
| $N_2m_2$ | 1.08 | 0.94 | 0.55 | 62.29 | U:0.5-500 |

**S5.3 Pairwise population modeling of recent gene flow with ABC**

We implemented an ABC approach to estimate the probability of recent gene flow (53) between Apennine and European brown bear populations. We developed a demographic model where an ancestral population of effective size *Na* splits at time *Tdiv* in two populations of size *N1* and *N2*. These two populations exchange migrants at rates *m12* and *m21* until time *Tmig,* and after that time they become completely isolated. We considered two pairs: Apennine vs. Alps, using the Alps as the closest source or target of gene flow for the Apennine population, and Alps vs. Slovakia as a control. Prior distributions are reported in Table S7.

We used *ms* (39) to generate 1 million simulations drawing demographic parameter combinations according to the prior distributions. When *Tmig* is 0, the model allows migration since divergence until present time; when *Tmig* equals *Tdiv,* the model converges to divergence without migration. In each simulation, we generated 4,000 independent loci of 2,000 bp using a mutation rate of $1.82 \times 10^{-8}$ per generation and no intra locus recombination, sampling 2 chromosomes for each population. The four moments of the distribution of private segregating sites in each population, of the shared polymorphisms

and of the fixed differences were used as summary statistics (53). A random sample of 2,000 bp-long 4,000 neutral loci genotyped in the high coverage Apennine (APN2), Alpine (ALP1), and Slovakian (SLK1) individuals were used to compute the observed values for the selected summary statistics.

The non-linear regression approach based on neural networks from the *abc R* package (38) was used to estimate the posterior distribution of the seven demographic parameters of the model, retaining 1% of the simulations closest to the observed data with time scaled in years using a generation time of 11 years.

Mode and credible interval for the parameters are reported in Table S8. The best estimate for the time since isolation (*Tmig*) of the Apennine bear from the Alps is around 2,500 years ago, with a lower 2.5% support limit of approximately 1,700 years (SI Appendix, Table S8). When the same approach is used to compare the Alpine with the Slovakian genomes (a control with similar geographic distance in Southern Europe), we obtained a slightly larger estimate of *Tmig* of approximately 4,000 years (lower limit of about 2,500 years). This new analysis is clearly assuming a simplified two-populations model (as compared to the meta-population model in Section 5.2) and assumes a constant migration rate after the split and before a total isolation, but it clearly supports fragmentation with zero migration in the last few thousand years between groups separated by some hundred kilometers.

**Table S7. Prior distributions of ABC pairwise population modeling.** Population sizes are in number of diploid individuals and times in generations. U: uniform distribution, LU: log-uniform distribution.

| Parameter | Apennine vs. Alpine | Alpine vs. Slovakian |
|---|---|---|
| N1 | U:{10 – 3,000} | U:{10 – 100,000} |
| N2 | U:{10 – 100,000} | U:{10 – 100,000} |
| NA | U:{10-100,000} | U:{10-100,000} |
| Tmig | U:{0 – 5,000} | U:{0 – 5,000} |
| Tdiv | Tmig + U:{0 – 15,000} | Tmig + U:{0 – 15,000} |
| m12 | LU:{$10^{-5}$ – 0.2} | LU:{$10^{-5}$ – 0.2} |
| m21 | LU:{$10^{-5}$ – 0.2} | LU:{$10^{-5}$ – 0.2} |

**Table S8. Estimated parameters in the ABC pairwise population model.** Population sizes are in number of diploid individuals and times in years, assuming a generation time of 11 years. [a]Upper and lower limits of the 95% credible interval of the posterior distribution.

| | APN2 vs. ALP1 | | | ALP1 vs. SLK1 | | |
|---|---|---|---|---|---|---|
| | **0.025[a]** | **Mode:** | **0.975[a]** | **0.025[a]** | **Mode** | **0.975[a]** |
| N1 | 285 | 434 | 718 | 4,521 | 5,321 | 7,665 |
| N2 | 4,608 | 5,858 | 11,152 | 3,957 | 4,680 | 6,705 |
| Na | 29,885 | 31,083 | 33,717 | 36,021 | 37,492 | 39,320 |
| **Tmig** | **1,669** | **2,555** | **6,897** | **2,554** | **3,955** | **7,142** |
| Tdiv | 30,783 | 36,690 | 69,464 | 42,700 | 59,518 | 160,136 |
| m12 | 0.00001 | 0.00017 | 0.00936 | 0.00001 | 0.00013 | 0.06294 |
| m21 | 0.00001 | 0.00001 | 0.01552 | 0.00001 | 0.00032 | 0.07502 |

**S5.4 Estimation of Apennine brown bear divergence using *F***

Using the same statistical approach employed to date the interruption of gene flow between modern humans and Neandertals (55), we estimated the time since complete isolation of the Apennine population (ingroup 1) from the Central European population (ingroup 2). Alternatively using the brown bear sample from the Alps or from Slovakia as a representative of the European population, we counted the number of polymorphisms (i.e., heterozygous sites) in the European individual for which an allele sampled at random from the Apennine individual was the derived one (*F*). As we were only interested in novel substitutions occurred along the lineage leading to the Central European sample, the polar and the black bear sequences were used to polarize all polymorphisms (outgroups). Using the scaffold1 sequence and 10 replicates, ca. 70,000 and 75,500 polymorphic sites were found in the individuals from Alps and Slovakia, respectively, and for an average of 33.5% and 33.8% of them the derived allele was sampled at random in the Apennine individual (Fig. S15).

To translate from *F* to time since population divergence, a calibration curve was built employing coalescent-based simulations. Using the software *ms* (39), we designed a demographic model where two populations diverged some time in the past. Before the split, the demography was modelled as reconstructed by the PSMC analysis: a constant size population of 30,000 individuals started to decrease in size 10,000 generations ago to reach 2,000 individuals 1,000 generations ago. Then, the size remained constant until

the split. After the split, the effective population size of ingroup 2 was modelled as constant until present. The calibration curve was built setting the time since divergence from 100 to 900 generations in the past (100 generations steps) and the ingroup 2 extant population size from 1000 to 4000 individuals. It is important to note that *F* has been shown to be insensitive to ingroup 1 population history as long as the lineage leading to this population did not exchange genes with other populations on the ingroup 2 lineage. We ran 20 replicates per each combination of these parameters (Fig. S16).

**Figure S15. Simulated and real *F* values to estimate Apennine population divergence.** Coalescent-based simulations of the proportion of polymorphisms in the Central European population for which the derived allele (*F*) is found in the Apennine population for different time since divergence of the two populations and different estimates of the extant size ($N_e$) of the Central European population. The observed *F,* estimated over ten replicates on scaffold 1 sequence and using the Slovak (green) or the alpine (red) individual as representative of the Central European population, is shown in the inset. Mean observed estimates of *F* are also given in the main plot as horizontal lines. The sample size for the Apennine brown bear sample in the simulations is equal to one haploid genome.

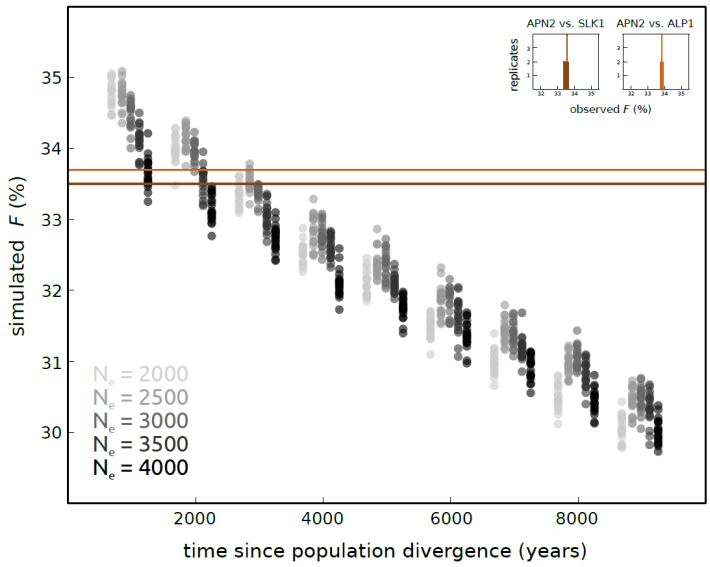

**S6 Mitochondrial Neighbor-Joining tree**

In order to reconstruct the mtDNA phylogeny of brown bears, all the raw reads belonging to each individual were merged and mapped against a whole mitochondrial genome following the same bioinformatic protocol as for the whole genome mapping (see Section S1.3-1.4). In particular, a mtDNA haplotype from France (GenBank: EU497665, 16,753bp) was used as reference genome for the 14 brown bears and an *U. maritimus* haplotype (GenBank: AP012596, 16,971bp) for the six polar bears. To increase the sample size of the mitochondrial dataset, one Illumina MiSeq lane (2x75bp kit) was used to sequence 11 additional samples: six brown bears from the Apennine, three from Slovakia and two from Greece, producing ~20 million paired-end reads. The raw reads of these additional samples were processed using the same procedure detailed above and the mean coverage for each of the 31 individuals in this extended dataset is reported in Table S9. Geneious v8.0.3 (56) was used to import bam alignments, extract a consensus sequence (majority rule) for each individual and masking nucleotides having a phred base quality < 20. The consensus sequences were then aligned using the MAFFT (57) plug-in in Geneious, adding the *U. americanus* haplotype (GenBank: JX196366.1, 16,434bp) as outgroup. The resulting alignment was manually inspected in order to identify and remove regions containing alignment errors, leading to a final length of 16,409bp. Based on this alignment, a Neighbor-Joining tree was built using Geneious computing the distance between individuals with the HKY nucleotide substitution model. The Neighbor-Joining tree based on mtDNA distances is shown in Figure 1 in the main text.

**Table S9**. **Samples employed in the mitochondrial Neighbor-Joining tree reconstruction**. GenBank accession number is provided for whole mitochondrial genome sequences produced in this study. Genome sequences downloaded from public repository and referenced in previously published studies are indicated. No brown bears from America were used to avoid possible admixture issues (10).

| Sample ID | Color code | Accession/ Reference | Species | Origin | Coverage |
|---|---|---|---|---|---|
| APN1 | | MF593979 | *U. arctos* | Central Italy | 24.8 |
| APN2 | | MF593975 | *U. arctos* | Central Italy | 84.9 |
| APN3 | | MF593973 | *U. arctos* | Central Italy | 21.2 |
| APN4 | | MF593972 | *U. arctos* | Central Italy | 43.3 |
| APN5 | | MF593971 | *U. arctos* | Central Italy | 27.9 |
| APN6 | | MF593970 | *U. arctos* | Central Italy | 27.1 |
| apn7 | | MF593978 | *U. arctos* | Central Italy | 3.3 |
| apn8 | | MF593977 | *U. arctos* | Central Italy | 4.1 |
| apn9 | | MF593976 | *U. arctos* | Central Italy | 3.5 |
| apn10 | | MF593974 | *U. arctos* | Central Italy | 5 |
| apn11 | | MF593969 | *U. arctos* | Central Italy | 3.8 |
| apn12 | | MF593968 | *U. arctos* | Central Italy | 46.7 |
| GRE1 | | MF593967 | *U. arctos* | Greece | 91.5 |
| GRE2 | | MF593966 | *U. arctos* | Greece | 103.8 |
| gre3 | | MF593965 | *U. arctos* | Greece | 12.9 |
| gre4 | | MF593964 | *U. arctos* | Greece | 10.7 |
| SLK1 | | MF593961 | *U. arctos* | Slovakia | 98.9 |
| SLK2 | | MF593960 | *U. arctos* | Slovakia | 66.6 |
| slk3 | | MF593963 | *U. arctos* | Slovakia | 50.9 |
| slk4 | | MF593962 | *U. arctos* | Slovakia | 61.4 |
| slk5 | | MF593959 | *U. arctos* | Slovakia | 73.8 |
| SPA1 | | MF593958 | *U. arctos* | NW Spain | 71.5 |
| ALP1 | | MF593957 | *U. arctos* | N Italy | 42.5 |
| SWE1 | | grz3 (11) | *U. arctos* | S Sweden | 702.2 |
| SWE2 | | grz4 (11) | *U. arctos* | N Sweden | 537.2 |
| POL1 | | pb28 (11) | *U. maritimus* | E Greenland | 402.2 |
| POL2 | | pb7a (11) | *U. maritimus* | E Greenland | 91.5 |
| POL3 | | pb3 (12) | *U. maritimus* | E Greenland | 63.1 |
| POL4 | | pb105 (11) | *U. maritimus* | W Greenland | 43.3 |
| POL5 | | pb12 (11) | *U. maritimus* | W Greenland | 340.1 |
| POL6 | | pb68 (11) | *U. maritimus* | W Greenland | 601.3 |

**S7. Y-chromosome genetic diversity and structure**

Sex-biased dispersal due to higher mobility of males as compared with females is common among mammals and has also been suggested in the brown bear (17). To further test this hypothesis, we analyzed the genetic diversity and structure of scaffolds belonging to the Y-chromosome and compared the results with the genetic structure of the mitochondrial genome. In addition to all male individuals included in our dataset (Apennine: 3, Slovakia: 2, Greece: 2, and Spain: 1; see Table S1), we downloaded the raw sequencing reads of 19 male individuals (see Table S10) available in public repositories (10-12) and processed them through the same bioinformatic protocol outlined in Section S1.3-1.4 to perform reads quality filtering and mapping to the Polar bear reference genome. We restricted our analyses to two scaffolds of the Polar bear reference genome located on the Y-chromosome (58) which were analyzed in (17): Scaffold 318 and 579. In this case, we jointly called the polymorphisms using *FreeBayes* (59) with minimum mapping quality = 30, minimum base quality = 20 and ploidy = 1. Polymorphisms in each individual were then used to reconstruct the haploid sequence for each scaffold in each individual using *vcf2fasta* in the *vcflib* package *(*https://github.com/vcflib/vcflib*)*. Microsatellite, indels, low coverage, too high coverage and missing data were masked in each individual sequence using *BedTools maskfasta* (60) before any downstream analyses. Novel partial Y-chromosome scaffold 318 and scaffold 579 sequences produced in this study have been made publicly available in GenBank: Acc. Num. MF593980 (APN2), MF593981 (APN3), MF593982 (APN5), MF593983 (GRE1), MF593984 (GRE2), MF593985 (SLK1), MF593986 (SLK2), MF593987 (SPA1).

Nucleotide sequences of the haplotypes presented in (17) were downloaded from NCBI database (3.1Kb from Scaffold 318 sequenced in 128 individuals and 2.2Kb from Scaffold 579 in 63 individuals; see Table S11). All sequences (whole scaffold sequences for re-sequenced samples and short sequences for haplotypes in (17) were aligned to each other using MAFFT (57). The final dataset included 5.3 Kb-long sequences for 155 male individuals. *DNAsp* (61) and *TCS* (62) were used to reconstruct a Weighted Neighbor Joining network as (17).

Our results (Fig. S17) are consistent with those obtained in (17): one common haplotype was found across the entire brown bear range with the addition of few other haplotypes which were on average one substitution apart from the common haplotype and present in only one or two individuals. All Apennine male individuals share a haplotype (BR1.4) with one substitution difference from the most common brown bear haplotype (BR1.1). Male individuals from Spain and Greece have the common BR1.1 haplotype whereas the male individuals from Slovakia show a distinct haplotype (BR1.5) with one substitution difference from the most common brown bear haplotype (BR1.1). According to (17), male-specific dispersal could explain this pattern. A slower substitution rate of the Y in comparison with autosomal or mitochondrial chromosomes has also been proposed as an alternative or complementary explanation (63).

Considering that genetic variation at the Y-chromosome region analyzed in this merged data set is low, and this might have an impact in the inferred low geographic structure, we also used 600kb of the Y-chromosome from Apennine and Slovakia males in our study to estimate a Hudson-Fst metric that takes into consideration between and within groups genetic variation. We compared estimates of $F_{ST}$ between the two longest Y-chromosome scaffolds (297 and 318) with the whole mitochondrial genome in the male individuals in our study: 3APN, 2 GRE, and 2SLK. Haploid Y-chromosome sequences were retrieved in ANGST (21) using the most frequent base. Only sites with no missing data across all male individuals were used. We found very different values of $F_{ST}$ in Y-chromosome (0.05) and mitochondrial (0.98) loci, further supporting the hypothesis of sex-biased dispersal in the brown bear.

**Table. S10. Whole genome samples downloaded from public repositories and included in the Y-chromosome analysis**

| Sample ID | Reference | Species | Origin |
|---|---|---|---|
| ABC01 | (11) | *Ursus arctos* | Alaska, US |
| ABC2 | (12) | *Ursus arctos* | Alaska, US |
| ABC03 | (11) | *Ursus arctos* | Alaska, US |
| ABC04 | (11) | *Ursus arctos* | Alaska, US |
| GP01 | (11) | *Ursus arctos* | Montana, US |
| PB40 | (11) | *Ursus maritimus* | E Greenland |
| PB25 | (11) | *Ursus maritimus* | E Greenland |
| PB8 | (12) | *Ursus maritimus* | Svalbard, Norway |
| PB10M | (12) | *Ursus maritimus* | Svalbard, Norway |
| PB45 | (11) | *Ursus maritimus* | W Greenland |
| PB47 | (11) | *Ursus maritimus* | W Greenland |
| PB10L | (11) | *Ursus maritimus* | W Greenland |
| PB79 | (11) | *Ursus maritimus* | W Greenland |
| JC004 | (10) | *Ursus maritimus* | Canada |
| AK1 | (12) | *Ursus maritimus* | Alaska, US |
| AK2 | (12) | *Ursus maritimus* | Alaska, US |
| AK3 | (12) | *Ursus maritimus* | Alaska, US |
| AK4 | (12) | *Ursus maritimus* | Alaska, US |
| BLK | (12) | *Ursus americanus* | Alaska, US |

**Table. S11. Partial haplotypes from (17) included in the Y-chromosome analysis.**

| Haplotype | n | bp | Species | Origin |
|---|---|---|---|---|
| BR1.1 | 4 | 5.3 Kb | *U. arctos* | Alaska, US |
| BR1.1 | 2 | 3.1 Kb | *U. arctos* | Alaska, US |
| BR1.1 | 1 | 5.3 Kb | *U. arctos* | Idaho, US |
| BR1.1 | 2 | 5.3 Kb | *U. arctos* | ABC islands, US (in front of) |
| BR1.1 | 10 | 5.3 Kb | *U. arctos* | ABC islands, US |
| BR5 | 1 | 5.3 Kb | *U. arctos* | ABC islands, US |
| BR1.1 | 7 | 3.1 Kb | *U. arctos* | N Europe |
| BR1.2 | 2 | 5.3 Kb | *U. arctos* | N Europe |
| BR1.3 | 1 | 5.3 Kb | *U. arctos* | N Europe |
| BR1.1 | 6 | 5.3 Kb | *U. arctos* | Central Europe |
| BR1.1 | 8 | 3.1 Kb | *U. arctos* | Central Europe |
| BR1.1 | 1 | 5.3 Kb | *U. arctos* | Ural Mountains, Russia |
| BR1.1 | 3 | 3.1 Kb | *U. arctos* | Ural Mountains, Russia |
| BR3 | 1 | 5.3 Kb | *U. arctos* | Ural Mountains, Russia |
| BR1.1 | 1 | 5.3 Kb | *U. arctos* | W Siberia, Russia |
| BR1.1 | 1 | 3.1 Kb | *U. arctos* | W Siberia, Russia |
| BR1.2 | 1 | 5.3 Kb | *U. arctos* | W Siberia, Russia |

| | | | | |
|---|---|---|---|---|
| BR1.1 | 13 | 3.1 Kb | *U. arctos* | Kamtchatka, Russia |
| BR1.1 | 10 | 5.3 Kb | *U. arctos* | Kamtchatka, Russia |
| BR2 | 1 | 5.3 Kb | *U. arctos* | Kamtchatka, Russia |
| BR1.1 | 2 | 3.1 Kb | *U. arctos* | E Russia |
| BR1.1 | 2 | 5.3 Kb | *U. arctos* | E Russia |
| BR1.1 | 8 | 3.1 Kb | *U. arctos* | Canada |
| PO1.1 | 5 | 5.3 Kb | *U. maritimus* | Alaska, US |
| PO1.1 | 11 | 3.1 Kb | *U. maritimus* | Alaska, US |
| PO1.1 | 4 | 3.1 Kb | *U. maritimus* | W Greenland |
| PO1.1 | 2 | 5.3 Kb | *U. maritimus* | W Greenland |
| PO1.1 | 1 | 5.3 Kb | *U. maritimus* | W Greenland |
| PO1.1 | 1 | 5.3 Kb | *U. maritimus* | E Greenland |
| PO1.2 | 1 | 5.3 Kb | *U. maritimus* | E Greenland |
| PO1.1 | 1 | 5.3 Kb | *U. maritimus* | Iceland |
| PO1.1 | 1 | 5.3 Kb | *U. maritimus* | Franz Josef Land |
| PO1.1 | 3 | 5.3 Kb | *U. maritimus* | Davis Strait |
| PO1.1 | 6 | 3.1 Kb | *U. maritimus* | Davis Strait |
| BL1 | 1 | 5.3 Kb | *U. americanus* | Montana, US |

| | | | | |
|---|---|---|---|---|
| BL1 | 1 | 5.3 Kb | *U. americanus* | Oregon, US |
| BL2 | 1 | 5.3 Kb | *U. americanus* | Alaska, US - zoo |
| BL2 | 1 | 5.3 Kb | *U. americanus* | Vermont, US |

**Figure S16. Weighted Joining haplotype network of 5.3 kb sequences from Y-chromosome Scaffold 318 and scaffold 579.** The eight males in this study have BR1.4 (red, Apennines), BR1.1 (yellow, Spain; green, Greece) and BR1.5 (light brown, Slovakia). Whole-genome samples downloaded from public repositories (Table S10) cluster with the haplotypes described in (17) with the exception of one polar bear from Alaska (haplotype PO3) and the black bear (haplotype BL3). Color codes are consistent with the previous figures and tables. The geographic location of each haplotype from (17) is reported in Table S11.

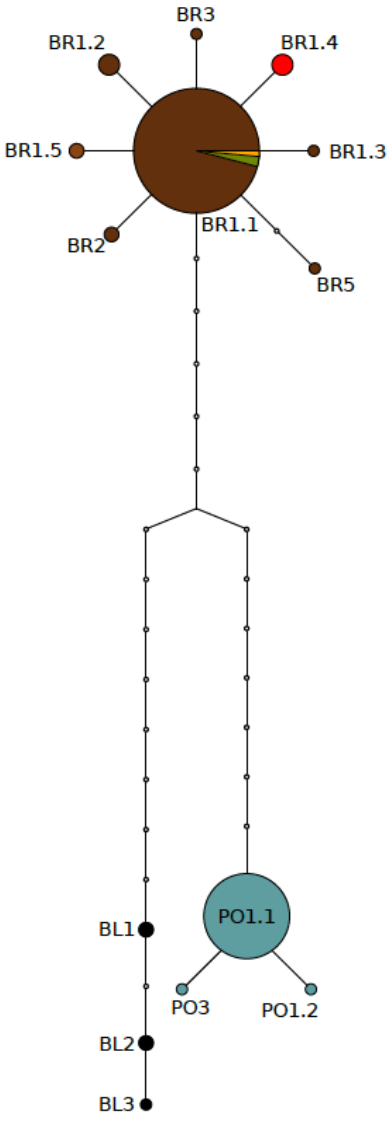

## S8 Detecting high variation regions in the Apennine brown bear genome

### S8.1 Genomic retention of non-synonymous SNPs

In the coding region, we selected all heterozygous sites in a single non-Apennine "reference" individual genotyped at high coverage, and we categorized them in non-synonymous (n-syn) and synonymous (syn) sites. We then estimated the fraction of the same sites that were also polymorphic in the five Apennine samples, for syn and n-syn sites separately ($P_{n\text{-}syn}$ and $P_{syn}$). Assuming that heterozygous sites in the reference genome are a proxy of the polymorphism in the Apennine ancestral population, $P_{n\text{-}syn}$ and $P_{syn}$ are estimates of the probability to retain a polymorphism during the Apennine population divergence. This is a McDonald-Kreitman-like test (64) on all genes during the Apennine population divergence. We predict that $P_{n\text{-}syn}$ and $P_{syn}$ should be the same if drift is mainly driving the fixation of non-synonymous substitution in the Apennine brown bear genomes. However, if balancing selection played an important role during the divergence of the Apennine brown bear, we predict that $P_{n\text{-}syn}$ should be higher than $P_{syn}$. On the contrary, if directional selection is a major force, we expect that $P_{n\text{-}syn}$ should be lower than $P_{syn}$. Results obtained using either the ALP1 or the SLK1 high coverage genomes as the "reference" individual for the genomic variation before the isolation of the Apennine population are reported in Table S12. Independently of the "reference" individual, the fraction of retained polymorphisms in the Apennine brown bear is higher for the non-synonymous ($P_{n\text{-}syn}$) compared to the synonymous ($P_{syn}$) sites.

A possible weakness of this analysis depends on the fact that heterozygous sites in the "reference" individual probably have different frequency distribution (in the reference population) at non-synonymous compared to synonymous variants, with more intermediate frequencies expected at synonymous variants. This effect, however, predict a more likely fixation by drift in the derived Apennine group at non-synonymous variants, which is the opposite of our observations. On the other hand, we might expect that a global pattern of retention of genetic variation during population divergence (i.e., incomplete lineage sorting) is more likely for non-synonymous variants due to balancing selection, especially without strong positive selection. In other words, the higher fraction of segregating sites at non-synonymous variants observed in Table S12 could be a general process in the divergence of any population, and not a specific case for the Apennine brown bear population. To test this hypothesis, we applied the same analyses as in Table S12, using again the ALP1 and SLK1 as "reference" individuals, but using the Slovakian and the Greek pairs of genomes (Table S13) as test control. We also repeated the analysis for the Apennine population, but using only two (randomly) selected individuals to analyze the same sample size as for Slovakia and Greece (similar results are obtained using different Apennine individuals). The fraction of sites which are heterozygous in the "reference" individual (either ALP1 or SLK1) and are also segregating in the pairs of Slovakian or Greek samples is only slightly higher for non-synonymous than synonymous sites, possibly suggesting an overall slightly higher tendency to incomplete lineage sorting at non-synonymous sites. On the contrary, as observed also in Table S12, this fraction is about one third higher for non-synonymous compared to synonymous sites when a pair of Apennine individuals is analyzed, supporting the hypothesis that the Apennine brown bear genomes are consistently affected by balancing selection that preserves non-synonymous variation.

**Table S12**. **Estimated probabilities to retain ancestral polymorphisms in the Apennine brown bear genomes**. The fractions of heterozygous sites in a "reference" genome (ALP1 or SLK1) that are polymorphic or fixed in the 5 Apennine brown genomes are separately computed for n-syn ($P_{n\text{-}syn}$) and syn ($P_{syn}$) sites.

| "Reference" genome | # heterozygous sites in the reference | n-syn (fixed/polymorphic in the Apennine individuals) | syn (fixed/polymorphic in the Apennine individuals) | $P_{n\text{-}syn}$ | $P_{syn}$ | $\chi^2$ (p-value) |
|---|---|---|---|---|---|---|
| ALP1 | 32373 | 15217 (9004/6213) | 17156 (11919/5237) | 0.41 | 0.31 | 374.1 ($<10^{-10}$) |
| SLK1 | 29499 | 13987 (8554/5433) | 15512 (10905/4607) | 0.39 | 0.30 | 273.5 ($<10^{-10}$) |

**Table S13**. **Control for the inference in Table S12**. The estimated probabilities are computed as in Table S12, but the $P_{n\text{-}syn}$ and $P_{syn}$ fraction are computed using two Apennine, two Slovakian and two Greek individuals, respectively.

| Reference genome | Two APN | | SLK1+SLK2 | | GRE1+GRE2 | |
|---|---|---|---|---|---|---|
| | $P_{n\text{-}syn}$ | $P_{syn}$ | $P_{n\text{-}syn}$ | $P_{syn}$ | $P_{n\text{-}syn}$ | $P_{syn}$ |
| ALP1 | 0.34 | 0.25 | 0.55 | 0.54 | 0.54 | 0.52 |
| SLK1 | 0.36 | 0.26 | - | - | 0.54 | 0.51 |

**S8.2 Genomic windows at high variation: distribution and content**

We first analyzed the distribution of $\theta_W$ along the genome, by 50 kb overlapping windows (shift of 10kb), in the alignment of five non-Apennine brown bears (ALP1, SLK1, SLK2, GRE1, GRE2; same sample size as in the Apennine population). In this alignment, we identified the average windows (AveWi) and the top windows (TopWi), which are the 50kb windows with a $\theta_W$ within 10% of the global mean and with a $\theta_W$ higher than the 99$^{th}$ percentile, respectively (Fig. S17). We found 44,012 AveWi and 2,170 TopWi. We then analysed $\theta_W$ in the same windows but using the alignment of the five Apennine individuals. Only in 0.35% of the AveWi the Apennine individuals reach the average variation observed in the non-Apennine ones, but this fraction becomes 3.5% for the TopWi. In other words, maintenance of regions at high variation in the Apennine brown bear does not appear as a random process, but rather as an active process more likely to occur at specific regions where high variation is typical of the species.

The 76 TopWi regions in the Apennine brown bear span 1.76Mb of the autosomal scaffolds, and approximately 45 kb of them fall within the coding region. This fraction (2.5%) is almost twice as large as the overall fraction of coding sites in the genome (1.4%), thus supporting the idea that the maintenance of regions at high variation in related to a functional mechanism.

The software REACTOME (65, 66) suggests that the list of 87 genes found within the TopWi regions in the Apennine brown bear is significantly enriched by genes belonging to three main pathways and several sub-pathways (See Table S14). In particular, 6 genes related to the Adaptive Immune System (UBR4; IGLV4-60; HLA-DQA1; HLA-DQB1; HLA-DRB5; HLA-DRB1), 39 genes related to the Olfactory Signaling pathways (OR13C8; OR8A1; OR4C3; OR14C36; OR14A16; OR5A2; OR2T27; OR2L13; OR4C11; OR6F1; OR6C68; OR14K1; OR6C2; OR6M1; OR7A5; OR6C3; OR6C6; OR6K6; OR4D6; OR4A16; OR12D3; OR4A15; OR4C13; OR4C16; OR10X1; OR2K2; OR2T4; OR1G1; OR10R2; OR4C5; OR6C70; OR14A2; OR7E24; OR4S2; OR2AG1; OR4C45; OR7A10; OR10G6; OR7G2), and 2 genes related to the Digestion of Dietary Carbohydrate (AMY1B; AMY2B). The immune system is well known to be under balancing selection (e.g.,(67)), and the same selective force has been proposed for the olfactory receptors(68).

**Figure S17. Schematic representation of the criteria used to select average $\theta_w$ windows (AveWi) and top $\theta_w$ windows (TopWi).**

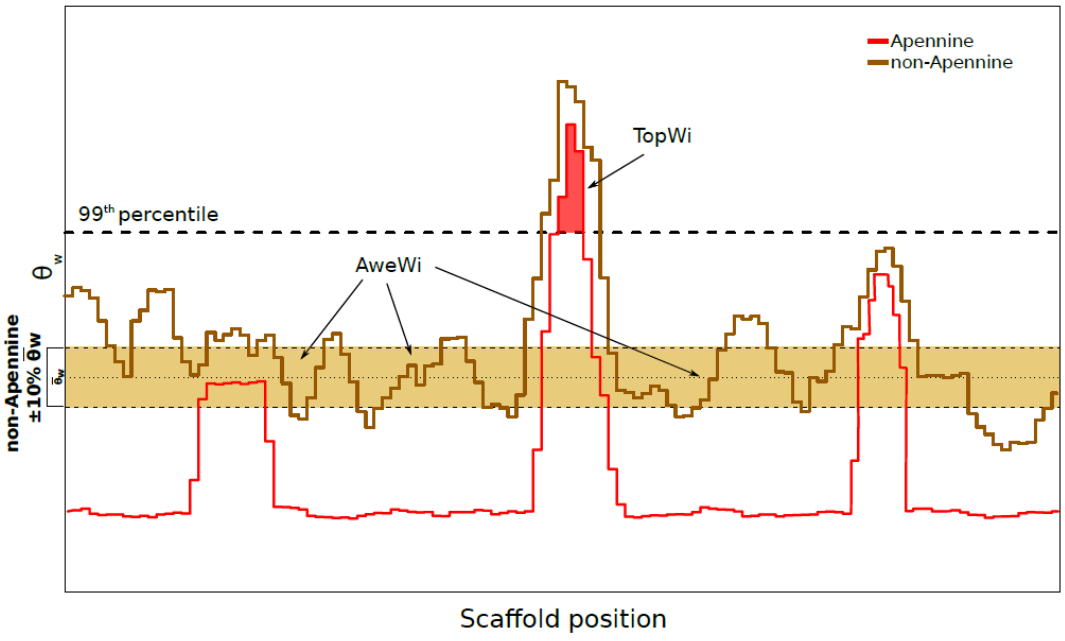

**Table S14. Enriched pathways in high variation regions.** Pathways and sub-pathways identified by Reactome as significantly more represented in the list of TopWi genes in the Apennine brown bear, compared to random expectation. Several *p*-values (corrected for multiple testing) are identical due to rounding of the floating point arithmetic in the software.

| Pathways and sub-pathways | p-value |
|---|---|
| Immune System | NS |
| Adaptive Immune System | $1.1E^{-3}$ |
| TCR Signaling | $<6.7E^{-16}$ |
| Generation of second messenger molecules | $<6.7E^{-16}$ |
| Translocation of ZAP-70 to immunological synapse | $<6.7E^{-16}$ |
| Downstream TCR signaling | $<6.7E^{-16}$ |
| Phosphorylation of CD3 and TCR zeta chains | $<6.7E^{-16}$ |
| Co-stimulation by the CD28 Family | $<6.7E^{-16}$ |
| PD-1 signaling | $<6.7E^{-16}$ |
| MHC class II Antigen Presentation | $6.7E^{-16}$ |
| Cytokine Signaling in Immune System | $4.4E^{-4}$ |
| Interferon Signaling | $5.9E^{-14}$ |
| Interferon gamma signaling | $3.2E^{-10}$ |
| Signal Transduction | $3.0E^{-6}$ |
| Signaling by GPCR | $<6.7E^{-16}$ |
| GPCR Downstream Signaling | $<6.7E^{-16}$ |
| Olfactory signaling pathway | $<6.7E^{-16}$ |
| Metabolism | NS |
| Metabolism of Carbohydrates | NS |
| Digestion of Dietary Carbohydrate | $6.3E^{-6}$ |

**S8.3 Sanger sequencing at MHC loci**

Additional evidence supporting the hypothesis that balancing selection prevented loss of variation at important functional genes in the Apennine brown bear arises from Sanger sequencing of two MHC class II exons in DQB and DRB loci in 18 individuals from different areas. Primers were designed based on Goda et al. (69), Kuduk et al (70), and also considering our high coverage genomes around the genomic region identified as putative DRB or DQB by mapping the MHC class II DRB allele Urar-DRB*1 sequence and Urar-DQB*01 sequence from Kuduk et al (70).

The sequences of the primers are as follows:
DRB_F: 5' TTCACCAACGGCACGGAGC 3'
DRB_R: 5' ACCCCGTAGTTGTGTCTGC 3'
DRB sequence length: 180 bp
DQB_F: 5' AGGATTTCGTGCTCCAGTTTAAG 3'
DQB_R: 5' TCCTCAATCTGGTAGTTGTGTCT 3'
DQB sequence length: 225

PCR amplification of these loci was performed as described in (71). Each visible polymorphism was called, even if the peaks were very different in height. In order to avoid biases related to the possible presence of multiple copies of these genes (69), we estimated the level of variation simply counting the number of polymorphic sites. The number of segregating sites in the Apennine individuals is very close to that observed when different European samples (e.g. similar sample size) are considered together (Figure S18, first two columns in each histogram). When the Apennine samples are randomly sub-sampled to match the sample sizes from each European area, the number of segregating sites is similar, or even higher in some comparisons (Figure S19, last two columns in each histogram). It is interesting to note that the MHC variation in the Apennine bears is approximately nine tenth (DQB) and four fifth (DRB) than observed in the joint sample of non-Apennine individuals (from Greece, Slovakia, Alps, and Spain), whereas in the whole genome (and similarly in the coding fraction of the genome), the Apennine variation is about ⅓ than observed in the joint non-Apennine samples.

**Figure S18. Number of segregating sites at two MHC class II loci.** The number of chromosomes used in each comparison is reported on top of the bars. EUR (dark brown): all non-Apennine samples together. Labels and colors as in Table S1.

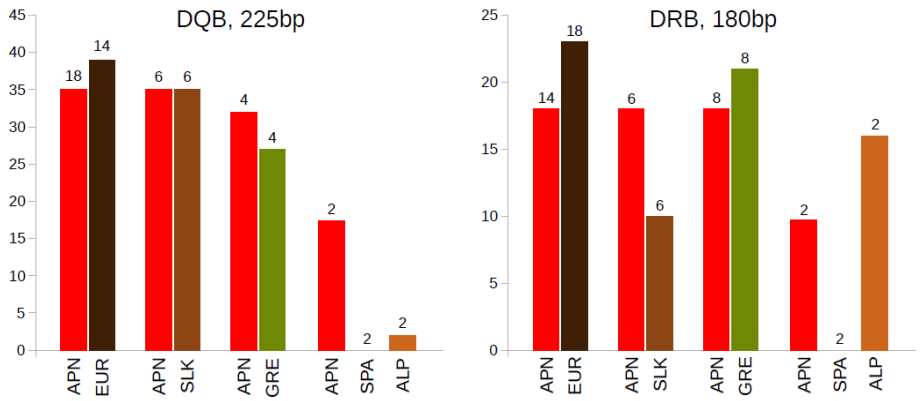

## S9. Fixed differences between Apennine and non-Apennine brown bear individuals

### S9.1 Nuclear genomes

The whole genome was screened for fixed differences, i.e. sites where all five Apennine genomes and all eight European (i.e., non Apennine) genomes are monomorphic for a different allele. This is an extreme version of the tests commonly applied to identify $F_{st}$ outliers (72). Such a test is required in our study as the small sample size of the Apennine population and the absence of a real homogenous European population for the comparison prevent allele frequencies estimations. This approach extracts sites subjected to a large shift during the Apennine population divergence, either by drift or by positive selection.

Approximately 1,000 fixed differences were found at 755 genes in the nuclear genome, and 411 in 360 genes implied non-synonymous substitutions. Among them, 40 were predicted as deleterious in the Apennine brown bear by two different bioinformatic tools (Panther (73) and Polyphen (74)), and none in the non-Apennine group. Four additional fixed mutations produced a premature stop codon (PSC) in the Apennine sample. Several loci were found to be directly related or associated to human pathologic phenotypes, as described in the following paragraphs (see the summary in Table S15).

#### S9.1.1 Mutations in genes causing monogenic human disorders

The OMIM database (Online Mendelian Inheritance in Man, Updated 20 April 2016) was used to identify relationships between human diseases and mutations in each of the 44 genes. Five genes showed a direct gene-human disease relationship: *RPS29* (OMIM: 615909 Diamond-Blackfan anemia - DBA); *COMP* (OMIM 177170, pseudoachondroplasia - PSACH; OMIM: 132400 multiple epiphyseal dysplasia-1 - EDM1), *LDB3* (OMIM: 601493, dilated cardiomyopathy-1C, left ventricular noncompaction-3, and familial hypertrophic cardiomyopathy-24; OMIM 609452 myofibrillar myopathy), *ADCK4* (OMIM: 615573, nephrotic syndrome type 9 - NPHS9), *ASL* (OMIM: 207900: Argininosuccinic aciduria). *RPS29* carries a PSC, while the first five genes carry a missense mutation.

The PSC mutation in *RPS29* truncates the ribosomal protein S29 after 32 amino acids, while the shortest functional isoform is 56 amino acid long (Ensembl ID: ENSG00000213741). RPS29 is a component of the small 40S ribosomal subunit and is essential for rRNA processing and ribosome biogenesis. Due to the PSC in homozygous state, in the Apennine brown bear RPS29 activity is completely abolished. Knockdown zebrafish rps19-/- show defective erythropoiesis and developmental abnormalities (75). In humans, RPS29 mutations cause DBA, an autosomal dominant disease with incomplete penetrance, that leads to severe anemia in the first year of life, increased frequency of cancer, and may include craniofacial anomalies such as flat nasal bridge, high arched or cleft palate, and short stature (76, 77).

Among the missense mutations, one is carried by the gene *COMP* directly related to a human disease affecting craniofacial morphology and body size. *COMP,* codes for an extracellular matrix protein that catalyzes the assembly of collagens and promotes formation of well-defined fibrils. Human mutations in this gene cause PSACH (more severe phenotype) or EDM1 (milder phenotype), both with dominant inheritance, characterized by disproportionate short stature, deformity of the lower limbs, brachydactyly, loose joints, and ligamentous laxity (78).

The *LDB3* gene encodes a PDZ-LIM domain-binding factor that plays an important role in maintaining the structural integrity of the striated muscle Z-disc in multiple species. Several mutations in this gene are associated with either cardiac and skeletal muscles related-diseases (79, 80). Two pathogenic mutations in humans have been identified few amino acids apart from the G200C amino acid mutation fixed in Apennine population (S196L rs45487699, T213I rs121908337), suggesting that this protein region is probably functionally important.

Finally, in humans, *ADCK4* is associated with a recessive chronic kidney disorder and *ASL* with a recessive metabolic disorder of the urea cycle, both leading to problems related to protein metabolism. Nephrotic syndrome type 9 caused by mutations in the *ADCK4* gene causes loss of protein through the kidneys (proteinuria) which leads to low protein levels in the blood (hypoalbuminemia). This may in turn cause water to be drawn into soft tissues (edema), and lead to chronic renal failure (81). Mutations in *ASL* gene coding for the enzyme argininosuccinate lyase causes the accumulation of argininosuccinic acid in the blood and urine that can affect the nervous system. This monogenic disorder, like other inborn errors of metabolism, manifests as a multifactorial disorder at the phenotypic level, including greater risk for poor neurocognitive outcome, hypertension, and liver disease (82).

**S9.1.2 Other categories**

Four missense mutations were carried by genes involved in immune response, host defense, and xenobiotic metabolism, and 10 by genes involved cell cycle, DNA or RNA-related processes. One of the 6 genes involved in specific metabolic pathways or inflammatory response, *SMPD2,* is part of the sphingolipid metabolic pathway, that plays a role in Type 2 Diabetes Mellitus (83), while *LDHB* causes lactate dehydrogenase-B deficiency (OMIM 614128). The latter may affect the ability of the cell to get energy directly from glucose through the lactic acid cycle impairing conversion of pyruvate into lactate. This metabolic cycle is particularly important in producing ATP during muscle activity. Three mutated genes encode for protein of structural or developmental importance. Among these, TET2 takes part in multiple processes and somatic mutation in its coding region cause an acute myeloid leukemia, called myelodysplastic syndromes in humans (OMIM 614286). Six additional genes are mainly involved in protein folding or metabolism (classified as "Other" in Table 17). The remaining 9 missense mutations and one a PSC, were carried by different olfactory receptor genes, all of them members of the largest coding gene superfamily in mammals (84).

**Table S15. Description of the nuclear deleterious mutations in the Apennine brown bear.**

| Gene name | Ensembl ID | AA position in polar bear | Description | Biological process | Molecular function | Phenotype (OMIM ID) |
|---|---|---|---|---|---|---|
| **Genes causing monogenic disorders in humans** | | | | | | |
| *COMP* | ENSP00000222271 | R36W XP_008702158.1 | cartilage oligomeric matrix protein | skeletal system development, growth plate cartilage development | protease binding, extracellular matrix structural constituent | EDM1 (177170), PSACH (132400) |
| *LDB3* | ENSP00000401437 | G200C XP_008694360.1 | LIM domain binding 3 | sarcomere organization | muscle alpha-actinin binding | CMD1C, LVNC3, CMH24 (601493) |
| *ADCK4* | ENSP00000315118 | R479H XP_008686942.1 | aarF domain containing kinase 4 | protein phosphorylation | protein serine/threonine kinase activity | NPHS9 (615573) |
| *ASL* | ENSP00000378741 | L216F XP_008696814.1 | argininosuccinate lyase | urea cycle | argininosuccinate lyase activity | argininosuccinic aciduria (207900) |
| *RPS29* (PSC[1]) | ENSP00000245458 | W32stop XP_008691789.1 | ribosomal protein S29 | nuclear-transcribed mRNA catabolic process, nonsense-mediated decay | structural constituent of ribosome | DBA13 (615909) |
| **Immune response, host defense, xenobiotic metabolism** | | | | | | |
| *DHRS2* | ENSP00000344674 | R210stop | dehydrogenase/reductase | response to toxic | oxidoreductase | |

| | | | | | | |
|---|---|---|---|---|---|---|
| (PSC)[1] | | XP_008708784 | (SDR family) member 2 | substance, cellular response to oxidative stress | activity | |
| *FCN1* | ENSP00000360871 | C33G XP_008707670.1 | ficolin 1 | complement activation, innate immune response, negative regulation of viral entry into host cell. | G-protein coupled receptor binding | |
| *CMA1* | ENSP00000250378 | R65W XP_008707035.1 | chymase 1, mast cell | multiple metabolic processes (e.g. angiotensin maturation, immune response) | serine-type endopeptidase activity | contributes to IgE responsiveness, atopic (147050) |
| *CYP2F1* | ENSP00000333534 | G88R XP_008686950.1 | cytochrome P450 family 2 subfamily F member 1 | xenobiotic metabolic process | monooxygenase activity | |

**Cell cycle, DNA or RNA-related processes**

| | | | | | | |
|---|---|---|---|---|---|---|
| *MMS19* | ENSP00000359818 | R717W XP_008700158.1 | MMS19 homolog, cytosolic iron-sulfur assembly component | DNA metabolic process, DNA repair | protein binding | |
| *DHX34* | ENSP00000331907 | P558L XP_008682862.1 | DEAH (Asp-Glu-Ala-His) box polypeptide 34 | RNA processing | nucleic acid binding | |
| *ZMYM1* | ENSP00000362427 | N576H XP_008692635.1 | zinc finger, MYM-type 1 | | nucleic acid binding, protein dimerization activity | |
| *CHAF1A* | ENSP00000301280 | A901V XP_008709485.1 | chromatin assembly factor 1 subunit A | DNA replication, chromatin assembly, cell cycle | chromatin binding | |
| *CEBPZ* | ENSP00000234170 | R473H XP_008698446.1 | CCAAT/enhancer binding protein (C/EBP), zeta | positive regulation of transcription from RNA polymerase II promoter | | |
| *ZNF780B* | ENSP00000391641 | R562Q XP_008686927.1 | zinc finger protein 780B | regulation of transcription, DNA-templated | nucleic acid binding | |
| *PARD3B* | ENSP00000385848 | A614T XP_008685773.1 | par-3 family cell polarity regulator beta | cell cycle | protein binding | |
| *MYCBP2* | ENSP00000444596 | R835C XP_008684900.1 | MYC binding protein 2, E3 ubiquitin protein ligase | transcription, DNA-templated | protein binding | |
| *FOXI1* | ENSP00000304286 | K245E XP_008690615.1 | forkhead box I1 | positive regulation of transcription, DNA-templated | | deafness (directly or via *SLC26A4* transcription control, 600791) |
| *ZNF177* | ENSP00000415070 | T615S XP_008703726.1 | ZNF559-ZNF177 readthrough | regulation of transcription, DNA-templated | nucleic acid binding | |

**Metabolism and inflammatory response**

| | | | | | | |
|---|---|---|---|---|---|---|
| *LDLR* | ENSG00000130164 | V720A XP_008709151.1 | low density lipoprotein receptor | Lipid metabolic process and transport | calcium ion, protein and glycoprotein binding | Hypercholesterolemia, familial (143890) |
| *SMPD2* | ENSP00000258052 | L314P XP_008704475.1 | sphingomyelin phosphodiesterase 2 | ceramide biosynthetic process | sphingomyelin phosphodiesterase activity | sphingolipid metabolic pathway plays a role in Type 2 Diabetes Mellitus |
| *LDHB* | ENSP00000229319 | G188R XP_008691336.1 | lactate dehydrogenase B | lactate/pyruvate metabolic process | lactate dehydrogenase activity | lactate dehydrogenase-B deficiency (614128) |
| *HRH4* | ENSP00000256906 | V122A | histamine receptor H4 | multiple processes (e.g. | G protein-coupled | |

| | | | | | | |
|---|---|---|---|---|---|---|
| | | XP_008689051.1 | | inflammatory response, synaptic transmission, cholinergic). | receptors | |
| *NOX1* | ENSP00000362057 | G412R XP_008699924.1 | NADPH oxidase 1 | angiogenesis, regulation of systemic arterial blood pressure by renin-angiotensin, inflammatory response | superoxide-generating NADPH oxidase activity | |
| *SULT6B1* | ENSP00000444081 | R140Q XP_008698774.1 | sulfotransferase family 6B member 1 | metabolic process | sulfotransferase activity | |

**Structural role and development**

| | | | | | | |
|---|---|---|---|---|---|---|
| *TET2* | ENSP00000425443 | L716I XP_008687609.1 | tet methylcytosine dioxygenase 2 | multiple processes (e.g. cell cycle, gene expression, kidney development, hemopoiesis) | methylcytosine dioxygenase activity | myelodysplastic syndromes (somatic mutations, 614286) |
| *KRT84* | ENSP00000257951 | S314L XP_008702829.1 | keratin 84, type II | hair follicle development, nail development | structural constituent of cytoskeleton | |
| *ISG20L2* | ENSP00000357202 | S279Q XP_008694768.1 | interferon stimulated exonuclease gene 20kDa like 2 | ribosome biogenesis. | nucleic acid and protein binding | |

**Other**

| | | | | | | |
|---|---|---|---|---|---|---|
| *PTPRT* | ENSP00000362294 | G1082S XP_008696473.1 | protein tyrosine phosphatase, receptor type T | protein dephosphorylation | | |
| *UBE4B* | ENSP00000343001 | D1101N XP_008692966.1 | ubiquitination factor E4B | ubiquitin-dependent protein catabolic process | | |
| *TTC1* | ENSP00000429225 | E201A XP_008690657.1 | tetratricopeptide repeat domain 1 | protein folding | | |
| *CAPN8* | ENSP00000401665 | L584R XP_008693630.1 | calpain 8 | proteolysis | | |
| *RIBC1* | ENSP00000364476 | R300H XP_008702479.1 | RIB43A domain with coiled-coils 1 | | protein binding | |

[1]PSC: premature stop codon

### S9.2 mtDNA genomes

The analysis described in S8.1 was performed on the mtDNA genome as well, comparing the Apennine population haplotype (shared by all the individuals) with 45 European sequences from public repositories and from our non-Apennine samples. In the case of the mtDNA, we looked for aminoacids fixed in the Apennine sequence and present in the non-Apennine group at low frequency (Table S16). The highest probability of being deleterious (P=0.78) was found for a gly>glu mutation in the NADH dehydrogenase subunit 5 (ND5) of mitochondrial complex I, with the glycine fixed in the non-Apennine brown group. Interestingly, the second and third highest P values are estimated for two additional ND5 mutations rare in the non-Apennine brown group. These specific mutations have not been described in human patients, but several ND5 changes have been shown to reduce the activity of complex I, reducing energy production within mitochondria and causing different health problems, including muscle weakness (85). The functional importance of the gly residue is supported by its level of conservation across vertebrates. We computed a BLAST search of the Apennine bear ND5 protein against the refseq protein database retrieving the first 500 hits of different taxonomic groups. The 526 gly residue is fixed in mammals and birds; fishes show a low-frequency conservative change (gly>ala in 9 out of 500 sequences). In reptiles and amphibians ala and gly have a similar frequency, but results are less informative because of the fewer -and often partial- sequences of these two groups in the database. The 526 mutation is located in the transverse helix of the

C-terminal region of ND5. This lateral helix coordinates conformational changes of other subunits of complex I (86), and may be directly involved in the control of the proton transfer events from the matrix to the inner membrane space ("piston role" (87)). Molecular evolutionary analyses in other vertebrates have shown signatures of positive selection and rapid evolution in this helix (88, 89), providing further support to the functional role of the ND5 lateral helix.

**Table S16. Deleterious mtDNA mutations in the Apennine brown bear.** Results of the Panther analysis on mtDNA mutations fixed in the Apennine brown sample but observed at low or 0 frequencies in a sample of 45 non-Apennine European brown bears and across vertebrates.

| Gene | Position | #APNs (out of 6) | #NonAPNs (out of 45) | Score | P_delet | P_wildtype | P_substituted |
|---|---|---|---|---|---|---|---|
| ND5 | G526E | 6 | 0 | -4.28 | 0.78 | 0.25 | 0.01 |
| ND5 | P447S | 6 | 5 | -3.59 | 0.64 | 0.17 | 0.03 |
| ND5 | T555A | 6 | 3 | -2.52 | 0.38 | 0.16 | 0.07 |
| CO3 | Y182H | 6 | 5 | -1.98 | 0.27 | 0.08 | 0.02 |
| ATP8 | S45P | 6 | 0 | -1.76 | 0.22 | 0.06 | 0.02 |
| ATP8 | S43P | 6 | 1 | -1.73 | 0.22 | 0.05 | 0.02 |
| CO2 | N117S | 6 | 1 | -1.59 | 0.20 | 0.04 | 0.07 |
| ATP8 | T36I | 6 | 7 | -1.41 | 0.17 | 0.05 | 0.02 |
| CYTB | A240T | 6 | 0 | -1.28 | 0.15 | 0.06 | 0.07 |
| ND2 | P123S | 6 | 5 | -0.64 | 0.09 | 0.12 | 0.12 |
| ND3 | V100A | 6 | 0 | -0.64 | 0.09 | 0.10 | 0.09 |
| ND4 | F256S | 6 | 5 | -0.45 | 0.07 | 0.06 | 0.07 |
| ND4 | N421D | 6 | 5 | -0.25 | 0.06 | 0.06 | 0.06 |

**S9.3 Enrichment of fixed differences in candidate genes for tame/aggressive behavior**

Although an exhaustive historical research has not been conducted yet, no cases of human casualties or attacks by wild Apennine bears have been reported to local authorities during the last century (90), http://www.parchionline.it/orso-bruno-in-italia.htm). Considering the proximity between bears and humans in the Central Apennines, especially in the core range of this population where several villages are located and thousands of visitors come every year, this absence of attacks suggests a much less aggressive behavior of Apennine bears compared to other European and worldwide brown bear populations (90).

Given the interesting behavioural differences suggested for the Apennine bear, we blindly tested if candidate genes previously associated in other mammals to tameness/aggressiveness show a higher than expected signal of genetic divergence in comparison with other brown bear populations. In particular, we selected 22 genes that recent genomic studies indicate as promising causative determinants of a recent shift from an aggressive to a more docile temperament. These association studies (see below) refer to the dog, pig, and yak domestication process, and to breed selection experiments for docile and aggressive behaviour in foxes and rats. Our criteria was to include in this analysis only the genes that were either

supported by independent studies, or that were considered as "plausible" by the Authors of the original paper.

Our list of TA (Tameness/Aggressiveness) genes included 22 items:

- *COUP-TFII*, *GABARAPL1*, and *GRIN2B*, identified from significant differences in allele frequencies between foxes selected for tame and aggressive behavior (91);
- *HTR2C*, which shows a significant expression difference between tame and aggressive foxes (92), between aggressive and nonaggressive rats (93), and is also associated with the fear behavior shift between wolf and dog (94);
- *GLTSCR2*, *LGI4*, *CYP7B1*, and *HTR3A*, identified as affecting brain gene expression in $F_2$ intercross of two outbred lines of rats selected for tame and aggressive behavior toward humans; in particular, *GLTSCR2* and *LGI4* satisfied a suite of different correlation criteria, including their map position within tameness QTL, and *CYP7B1* and *HTR3A* were considered as interested candidates with expression levels affected by trans-acting tameness QTL (95, 96);
- *TPH1* and *GABRA5*, considered as potential candidates explaining aggressiveness differences, and also identified with formal tests for positive selection for tameness and aggression in rats (97); *GABRA5* is also associated with the fear behavior shift between wolf and dog (94);
- *FGF13*, which shows a fixed difference between dogs and wolfs in a putatively functional segregating site, it is in a genomic region characterized by a strong signatures of dog-wolf divergence, and it was previously associated with the regulation of aggression behavior (98);
- *ARID3B, DCC, PLEKHH1*, *PCDHA1*, and *PCDHB4*, which are neural crest-related genes suggested to underlie the evolution of tameness during cat domestication (99); changes in neural-crest-derived tissues of behavioral relevance via multiple preexisting genetic variants were probably relevant during the initial selection for tameness in several species (100);
- *GNDF*, *DLL3*, and *DHDH*, which show differential expression in rats selected for high or low level of aggressiveness, and are possibly implicated in the mechanism underlying genetically defined aggressiveness (101, 102);
- *PLXNB1*, selected considering its potential role in the aggressive behavior in rats (95) and also found under selection during yak domestication (103);
- *GRM7* and *GRM8*, which are indicated as highly differentiated in pigs compared to wild boars, and have possibly played a critical role in the process of domestication that converts anxiety-associated aggressive behaviors of wild population to tame behavior in domestic animals (104).

Five of the 22 TA genes (*GABARAPL1*, *PCDHA1*, *PCDHB4*, *GNDF*, *DLL3*) were absent in the Polar bear reference genome whereas two mRNA annotated as *GRM8* were found and were both considered. For each of these 19 genes, we counted the number of sites with fixed differences between the five Apennine bears genomes and five non-Apennine bears in the Alps, Slovakia, and Greece, in a genomic region including the gene and two windows of 10 kb upstream and downstream the gene, respectively. When standardized by the total number of sites in the region (i.e. length), and averaged across genes, we obtain a $FD_{TA}$ (Fixed Differences in TA genes) equal to 0.000144 difference/site. This means that regions including candidate TA genes have on the average 0.14 sites every 1,000 bp where all the Apennine bears have the same nucleotide never observed in the reference non-Apennine brown bear group. In order to statistically verify if $FD_{TA}$ is larger than expected (i.e., if TA genes are enriched for fixed differences, possibly as a consequence of the fact that in the Apennine bears diverged from other brown bears at loci affecting the tameness/ aggressiveness behavior), we randomly sampled 10,000 groups of 19 genes and computed FD value for each random group. The distribution of random FD values is reported in Figure 1E in the main text, showing that $P(FD>FD_{TA}) < 0.05$. In other words, we found support for the hypothesis that Apennine bears are significantly different from other brown bears at a set of genes that in other studies were associated to differences between tame and aggressive individuals. The genes with higher than expected

proportion of fixed differences are: *HTR2C* (observed/expected fixed differences = 1.93), *GABRA5* (2.10), *GRM8* (2.13), *CYP7B1* (2.49), *DCC* (2.74), *GRM8* (3.13), *GLTSCR2* (3.14), *PLXNB1* (3.29), *GRM7* (15.05).

**S10. Supplementary references**


1. Ciucci P, et al. (2015) Estimating abundance of the remnant Apennine brown bear population using multiple noninvasive genetic data sources. *J Mammal* 96:206–220.
2. Ciucci P, et al. (2017) Distribution of the brown bear (*Ursus arctos marsicanus*) in the Central Apennines, Italy, 2005-2014. *Hystrix* 28:000–000. In press.
3. Morini et al (2017) Brown bears in Central Italy: a 15-year study on bear occurrence. *Europ Zool J* 84.1: 26–33.
4. Febbo D, Pellegrini M (1990) The historical presence of the brown bear in the Apennines. *Aquilo Ser Zool* 27: 85–87
5. Tosoni E, et al. (2017) Assessment of key reproductive traits in the Apennine brown bear (*Ursus arctos marsicanus*) population. *Ursus* 28:000–000. In press.
6. Gervasi V, et al. (2017) Estimating survival in the Apennine brown bear through multi-event modelling. *Population Ecology* 0:000–000. In press.
7. Swenson JE, Adamic M, Huber D, Stokke S (2007) Brown bear body mass and growth in northern and southern Europe. *Oecologia* 153:37–47.
8. Colangelo P, et al. (2012) Cranial distinctiveness in the Apennine brown bear: genetic drift effect or ecophenotypic adaptation? *Biol J Linn Soc Lond* 107:15–26.
9. Ciucci P, Tosoni E, Di Domenico G, Quattrociocchi F, Boitani L (2014) Seasonal and annual variation in the food habits of Apennine brown bears, central Italy. *J Mammal* 95:572–586.
10. Cahill JA, et al. (2015) Genomic evidence of geographically widespread effect of gene flow from polar bears into brown bears. *Mol Ecol* 24:1205–1217.
11. Liu S, et al. (2014) Population genomics reveal recent speciation and rapid evolutionary adaptation in polar bears. *Cell* 157:785–794.
12. Miller W, et al. (2012) Polar and brown bear genomes reveal ancient admixture and demographic footprints of past climate change. *Proc Natl Acad Sci USA* 109:E2382–E2390.
13. Meyer M, Kircher M (2010) Illumina sequencing library preparation for highly multiplexed target capture and sequencing. *Cold Spring Harb Protoc* 2010:db.prot5448.
14. Li H, Durbin R (2009) Fast and accurate short read alignment with Burrows-Wheeler transform. *Bioinformatics* 25:1754–1760.
15. Li H, et al. (2009) The Sequence Alignment/Map format and SAMtools. *Bioinformatics* 25:2078–2079.
16. McKenna A, et al. (2010) The Genome Analysis Toolkit: a MapReduce framework for analyzing next-generation DNA sequencing data. *Genome Res* 20:1297–1303.
17. Bidon T, et al. (2014) Brown and polar bear Y chromosomes reveal extensive male-biased gene flow within brother lineages. *Mol Biol Evol* 31:1353–1363.
18. GigaDB Dataset - DOI 10.5524/100008 - Genomic data from the polar bear (Ursus maritimus) Available at: http://gigadb.org/dataset/100008.
19. Danecek P, et al. (2011) The variant call format and VCFtools. *Bioinformatics* 27:2156–2158.
20. Kampstra P (2008) Beanplot: A boxplot alternative for visual comparison of distributions. *J Stat Softw* 28, Code Snippet 1.
21. Korneliussen TS, Albrechtsen A, Nielsen R (2014) ANGSD: Analysis of Next Generation Sequencing Data. *BMC Bioinformatics* 15:356.
22. Nielsen R, Paul JS, Albrechtsen A, Song YS (2011) Genotype and SNP calling from next-generation sequencing data. *Nat Rev Genet* 12:443–451.
23. Crawford JE, Lazzaro BP (2012) Assessing the accuracy and power of population genetic inference from low-pass next-generation sequencing data. *Front Genet* 3:66.

24. Korneliussen TS, Moltke I, Albrechtsen A, Nielsen R (2013) Calculation of Tajima's D and other neutrality test statistics from low depth next-generation sequencing data. *BMC Bioinformatics* 14:289.
25. Watterson GA (1975) On the number of segregating sites in genetical models without recombination. *Theor Popul Biol* 7:256–276.
26. Li H (2011) A statistical framework for SNP calling, mutation discovery, association mapping and population genetical parameter estimation from sequencing data. *Bioinformatics* 27:2987–2993.
27. Prüfer K, et al. (2014) The complete genome sequence of a Neanderthal from the Altai Mountains. *Nature* 505:43–49.
28. Jónsson H, et al. (2014) Speciation with gene flow in equids despite extensive chromosomal plasticity. *Proc Natl Acad Sci USA* 111:18655–18660.
29. Schubert M, et al. (2014) Prehistoric genomes reveal the genetic foundation and cost of horse domestication. *Partial haplotypes from (17) included in the Y-chromosome analysis*
30. Der Sarkissian C, et al. (2015) Evolutionary genomics and conservation of the endangered Przewalski's horse. *Curr Biol* 25:2577–2583.
31. Li H, Durbin R (2011) Inference of human population history from individual whole-genome sequences. *Nature* 475:493–496.
32. Beaumont MA, Zhang W, Balding DJ (2002) Approximate Bayesian computation in population genetics. *Genetics* 162:2025–2035.
33. Bertorelle G, Benazzo A, Mona S (2010) ABC as a flexible framework to estimate demography over space and time: some cons, many pros. *Mol Ecol* 19:2609–2625.
34. Maisano Delser P, et al. (2016) Population genomics of *C. melanopterus* using target gene capture data: demographic inferences and conservation perspectives. *Sci Rep* 6:33753.
35. Boitard S, Rodríguez W, Jay F, Mona S, Austerlitz F (2016) Inferring Population size history from large samples of genome-wide molecular data - An Approximate Bayesian Computation approach. *PLoS Genet* 12:e1005877.
36. Excoffier L, Dupanloup I, Huerta-Sánchez E, Sousa VC, Foll M (2013) Robust demographic inference from genomic and SNP data. *PLoS Genet* 9:e1003905.
37. Blum MGB, François O (2009) Non-linear regression models for Approximate Bayesian Computation. *Stat Comput* 20:63–73.
38. Csilléry K, François O, Blum MGB (2012) abc: an R package for approximate Bayesian computation (ABC). *Methods Ecol Evol* 3:475–479.
39. Hudson RR (2002) Generating samples under a Wright-Fisher neutral model of genetic variation. *Bioinformatics* 18:337–338.
40. Dumont BL, Payseur BA (2008) Evolution of the genomic rate of recombination in mammals. *Evolution* 62:276–294.
41. Vieira FG, Lassalle F, Korneliussen TS, Fumagalli M (2015) Improving the estimation of genetic distances from Next-Generation Sequencing data. *Biol J Linn Soc Lond* 117:139–149.
42. Paradis E, Claude J, Strimmer K (2004) APE: Analyses of Phylogenetics and Evolution in R language. *Bioinformatics* 20:289–290.
43. Pritchard JK, Stephens M, Donnelly P (2000) Inference of population structure using multilocus genotype data. *Genetics* 155:945–959.
44. Falush D, Stephens M, Pritchard JK (2003) Inference of population structure using multilocus genotype data: linked loci and correlated allele frequencies. *Genetics* 164:1567–1587.
45. Earl DA, vonHoldt BM (2011) STRUCTURE HARVESTER: a website and program for visualizing STRUCTURE output and implementing the Evanno method. *Conserv Genet Resour* 4:359–361.
46. Evanno G, Regnaut S, Goudet J (2005) Detecting the number of clusters of individuals using the software STRUCTURE: a simulation study. *Mol Ecol* 14(8):2611–2620.
47. Jakobsson M, Rosenberg NA (2007) CLUMPP: a cluster matching and permutation program for dealing with label switching and multimodality in analysis of population structure. *Bioinformatics* 23:1801–1806.
48. Chikhi L, Sousa VC, Luisi P, Goossens B, Beaumont MA (2010) The confounding effects of population

structure, genetic diversity and the sampling scheme on the detection and quantification of population size changes. *Genetics* 186:983–995.
49. Peter BM, Wegmann D, Excoffier L (2010) Distinguishing between population bottleneck and population subdivision by a Bayesian model choice procedure. *Mol Ecol* 19:4648–4660.
50. Eriksson A, Manica A (2014) The Doubly Conditioned Frequency Spectrum Does Not Distinguish between Ancient Population Structure and Hybridization. *Mol Biol Evol* 31:1618–1621.
51. Mazet O, Rodríguez W, Grusea S, Boitard S, Chikhi L (2015) On the importance of being structured: instantaneous coalescence rates and human evolution—lessons for ancestral population size inference? *Heredity* 116:362–371.
52. Gelman A (2004) Exploratory data analysis for complex models. *J Comput Graph Stat* 13:755–779.
53. Robinson JD, Bunnefeld L, Hearn J, Stone GN, Hickerson MJ (2014). ABC inference of multi-population divergence with admixture from unphased population genomic data. *Mol Ecol* 23: 4458–4471.
54. Brandvain Y, Kenney AM, Flagel L, Coop G, Sweigart AL (2014) Speciation and introgression between *Mimulus nasutus* and *Mimulus guttatus*. *PLoS Genetics* 10.6: e1004410.
55. Green RE, et al. (2010) A draft sequence of the Neandertal genome. *Science* 328:710–722.
56. Kearse M, et al. (2012) Geneious Basic: an integrated and extendable desktop software platform for the organization and analysis of sequence data. *Bioinformatics* 28:1647–1649.
57. Katoh K, Standley DM (2013) MAFFT multiple sequence alignment software version 7: improvements in performance and usability. *Mol Biol Evol* 30:772–780.
58. Bidon T, Schreck N, Hailer F, Nilsson MA, Janke A (2015) Genome-wide search identifies 1.9 Mb from the polar bear Y chromosome for evolutionary analyses. *Genome biol evol* 7.7: 2010–2022.
59. Garrison E, Marth G (2012). Haplotype-based variant detection from short-read sequencing. *arXiv preprint arXiv:1207.3907*.
60. Quinlan AR, Hall IM (2010) BEDTools: a flexible suite of utilities for comparing genomic features. *Bioinformatics 26*: 841–842.
61. Librado P, Rozas J (2009) DnaSP v5: a software for comprehensive analysis of DNA polymorphism data. *Bioinformatics* 25: 1451–1452.
62. Clement M, Posada DC, Crandall KA (2000) TCS: a computer program to estimate gene genealogies. *Mol ecol* 9: 1657–1659.
63. Nakagome S, Pecon-Slattery J, Masuda R (2008) Unequal rates of Y chromosome gene divergence during speciation of the family Ursidae. *Mol biol evol* 25: 1344-1356.
64. McDonald JH, Kreitman M (1991) Adaptive protein evolution at the Adh locus in Drosophila. *Nature* 351:652–654.
65. Fabregat A, et al. (2016) The Reactome pathway Knowledgebase. *Nucleic Acids Res* 44:D481–7.
66. Milacic M, et al. (2012) Annotating cancer variants and anti-cancer therapeutics in reactome. *Cancers* 4:1180–1211.
67. Hughes AL, Yeager M (1998) Natural selection at major histocompatibility complex loci of vertebrates. *Annu Rev Genet* 32:415–435.
68. Alonso S, López S, Izagirre N, de la Rúa C (2008) Overdominance in the human genome and olfactory receptor activity. *Mol Biol Evol* 25:997–1001.
69. Goda N, Mano T, Kosintsev P, Vorobiev A, Masuda R (2010) Allelic diversity of the MHC class II DRB genes in brown bears (*Ursus arctos*) and a comparison of DRB sequences within the family Ursidae. *Tissue Antigens* 76:404–410.
70. Kuduk K, et al. (2012) Evolution of major histocompatibility complex class I and class II genes in the brown bear. *BMC Evol Biol* 12:197.
71. Barbisan F, Savio C, Bertorelle G, Patarnello T, Congiu L (2009) Duplication polymorphism at MHC class II DRB1 locus in the wild boar (*Sus scrofa*). *Immunogenetics* 61(2):145–151.
72. Narum SR, Hess JE (2011) Comparison of FST outlier tests for SNP loci under selection. *Mol Ecol Resour* 11:184–194.

73. Thomas PD, et al. (2003) PANTHER: a library of protein families and subfamilies indexed by function. *Genome Res* 13:2129–2141.
74. Adzhubei IA, et al. (2010) A method and server for predicting damaging missense mutations. *Nat Methods* 7:248–249.
75. Danilova N, Sakamoto KM, Lin S (2008) Ribosomal protein S19 deficiency in zebrafish leads to developmental abnormalities and defective erythropoiesis through activation of p53 protein family. *Blood* 112:5228–5237.
76. Ball S (2011) Diamond Blackfan Anemia. *Hematology* 2011:487–491.
77. Mirabello L, et al. (2014) Whole-exome sequencing and functional studies identify RPS29 as a novel gene mutated in multicase Diamond-Blackfan anemia families. *Blood* 124:24–32.
78. Briggs MD, Chapman KL (2002) Pseudoachondroplasia and multiple epiphyseal dysplasia: mutation review, molecular interactions, and genotype to phenotype correlations. *Hum Mutat* 19:465–478.
79. Frank D, Kuhn C, Katus HA, Frey N (2006) The sarcomeric Z-disc: a nodal point in signalling and disease. *J Mol Med* 84:446–468.
80. Lin X, et al. (2014) Z-disc-associated, alternatively spliced, PDZ motif-containing protein (ZASP) mutations in the actin-binding domain cause disruption of skeletal muscle actin filaments in myofibrillar myopathy. *J Biol Chem* 289:13615–13626.
81. Ashraf S, et al. (2013) ADCK4 mutations promote steroid-resistant nephrotic syndrome through CoQ10 biosynthesis disruption. *J Clin Invest* 123:5179–5189.
82. Erez A (2013) Argininosuccinic aciduria: from a monogenic to a complex disorder. *Genet Med* 15:251–257.
83. Pralhada Rao R, et al. (2013) Sphingolipid metabolic pathway: an overview of major roles played in human diseases. *J Lipids* 2013:178910.
84. Buck LB (2000) The molecular architecture of odor and pheromone sensing in mammals. *Cell* 100:611–618.
85. Tuppen HAL, Blakely EL, Turnbull DM, Taylor RW (2010) Mitochondrial DNA mutations and human disease. *Biochim Biophys Acta* 1797:113–128.
86. Zhu J, Vinothkumar KR, Hirst J (2016) Structure of mammalian respiratory complex I. *Nature* 536:354–358.
87. Efremov RG, Baradaran R, Sazanov LA (2010) The architecture of respiratory complex I. *Nature* 465:441–445.
88. da Fonseca RR, Johnson WE, O'Brien SJ, Ramos MJ, Antunes A (2008) The adaptive evolution of the mammalian mitochondrial genome. *BMC Genomics* 9:119.
89. Garvin MR, Bielawski JP, Gharrett AJ (2011) Positive Darwinian selection in the piston that powers proton pumps in complex I of the mitochondria of Pacific salmon. *PLoS One* 6:e24127.
90. Naves J, et al. Brown bears attacks on humans in the world: a preliminary overview 2000-2015. 24th *International Conference on Bear Research and Management,* Anchorage, Alaska.
91. Johnson JL, et al. (2015) Genotyping-By-Sequencing (GBS) Detects Genetic Structure and Confirms Behavioral QTL in Tame and Aggressive Foxes (*Vulpes vulpes*). *PLoS One* 10:e0127013.
92. Kukekova AV, et al. (2011) Sequence comparison of prefrontal cortical brain transcriptome from a tame and an aggressive silver fox (*Vulpes vulpes*). *BMC Genomics* 12:482.
93. Popova NK, Naumenko VS, Kozhemyakina RV, Plyusnina IZ (2010) Functional characteristics of serotonin 5-HT2A and 5-HT2C receptors in the brain and the expression of the 5-HT2A and 5-HT2C receptor genes in aggressive and non-aggressive rats. *Neurosci Behav Physiol* 40:357–361.
94. Li Y, et al. (2014) Domestication of the dog from the wolf was promoted by enhanced excitatory synaptic plasticity: a hypothesis. *Genome Biol Evol* 6:3115–3121.
95. Heyne HO, et al. (2014) Genetic influences on brain gene expression in rats selected for tameness and aggression. *Genetics* 198:1277–1290.
96. Albert FW, et al. (2009) Genetic architecture of tameness in a rat model of animal domestication. *Genetics* 182:541–554.

97. Albert FW, et al. (2011) Targeted resequencing of a genomic region influencing tameness and aggression reveals multiple signals of positive selection. *Heredity* 107:205–214.
98. Cagan A, Blass T (2016) Identification of genomic variants putatively targeted by selection during dog domestication. *BMC Evol Biol* 16:10.
99. Montague MJ, et al. (2014) Comparative analysis of the domestic cat genome reveals genetic signatures underlying feline biology and domestication. *Proc Natl Acad Sci USA* 111:17230–17235.
100. Wilkins AS, Wrangham RW, Tecumseh Fitch W (2014) The "Domestication Syndrome" in Mammals: A Unified Explanation Based on Neural Crest Cell Behavior and Genetics. *Genetics* 197:795–808.
101. Ilchibaeva TV, Tsybko AS, Kozhemyakina RV, Popova NK, Naumenko VS (2016) Glial cell line-derived neurotrophic factor in genetically defined fear-induced aggression. *Eur J Neurosci* 44:2467–2473.
102. Albert FW, et al. (2012) A comparison of brain gene expression levels in domesticated and wild animals. *PLoS Genet* 8:e1002962.
103. Qiu Q, et al. (2015) Yak whole-genome resequencing reveals domestication signatures and prehistoric population expansions. *Nat Commun* 6:10283.
104. Moon S, et al. (2015) A genome-wide scan for signatures of directional selection in domesticated pigs. *BMC Genomics* 16:130.